Mechanical Analysis for US-APWR New and Spent Fuel Racks

Non-proprietary Version

March 2014

Revision History

Revision	Page	Description
0	All	Original issued
1		The following items were revised to incorporate results of the updated structural and mechanical analysis that was performed using the revised new and spent fuel rack structure and new five sets of time histories. Responses to RAIs 1032-7098 and 1054-7235 are incorporated as discussed below.
	P1	The cell wall thickness of SFR is changed.
	P1	The actual thickness of NFR of 0.209 inch is used in the analysis per the response to RAI 1032-7098 Question 09.01.02-29.
	P2	The explanation of the revised new and spent fuel rack structure is provided.
	P3,4,8	New five sets of time histories are used in the analysis per the responses to RAI 1054-7235 Question 09.01.02-43 and RAI 1032-7098 Questions 09.01.02-30, 31, and 32.
	P8,18	The computer code name is corrected per the response to RAI 1032-7098 Question 09.01.02-28.
	P16	A sensitivity run with the mixed loading condition is performed per the response to RAI 1032-7098 Question 09.01.02-33.
	P16	The random coefficients of friction are described in Tables 3-11 and 3-12 per the response to RAI 1032-7098 Question 09.01.02-34.
	P16-23 P23	Section 3.7 is updated to reflect analysis results. The effect of the thermal expansion issue on stress analysis is added per the response to RAI 1032-7098 Question 09.01.02-39.
	P24	The acceptance criterion for shallow drop is changed.
	P25	Justification is added for omitting results of the new fuel rack because the drop event for the new fuel rack is bounded by the drop event for the spent fuel rack
	P25	The analysis methods in Section 4.2 are modified.
	P27-28	Section 4.3 and 4.4 are updated to reflect the results.
	P29	The conclusions in Section 5.0 are updated.
	P30-31	The references in Section 6.0 are updated.

Revision	Page	Description
1	P32-34	Tables 2-1 through 2-3 are updated.
	P36-41	Tables 3-2 through 3-10 are updated.
	P42-43	Tables 3-11 and 3-12 are added per the response to RAI 1032-7098 Question 09.01.02-34.
	P44	Table 4-1 is updated.
	P44	Table 4-2 is added.
	P45-47	Figures 2-1 through 2-3 are updated.
	P54-69	Figures 3-8 through 3-23 are added.
	P73	Figures 4-4 through 4-5 are added.
	Various	Minor formatting and editorial corrections.

Mitsubishi Heavy Industries, Ltd.
16-5, Konan 2-chome, Minato-ku
Tokyo 108-8215 Japan

Abstract

This report considers the structural adequacy of the proposed US-APWR spent and new fuel racks under postulated loading conditions. Analyses and evaluations follow the U.S. Office of Technology Position paper and the NRC Standard Review Plan.
This report provides a discussion of the method of analyses, modeling assumptions, key evaluations, and results obtained to establish the margins of safety.

This report includes the following analysis results:

- Structural/Seismic Analysis
- Mechanical Accidental Analysis

It is confirmed that results of the above analyses satisfied the fuel racks requirements of the U.S. Office of Technology Position Paper and the NRC Standard Review Plan.

Table of Contents

List of Tables

List of Figures

List of Acronyms

ASME	American Society of Mechanical Engineers
B&PV	Boiler and Pressure Vessel
COF	Coefficient of Friction
DFR	Damaged Fuel Racks
DOF	Degree of Freedom
DFAC	Damaged Fuel Assembly Container
MHI	Mitsubishi Heavy Industries, LTD.
NFP	New Fuel Pit
NFR	New Fuel Racks
NOR	Number of Racks
NRC	Nuclear Regulatory Commission
OBE	Operating Basis Earthquake
OT	Office of Technology
QA	Quality Assurance
RG	Regulatory Guide
SFP	Spent Fuel Pit
SFR	Spent Fuel Racks
SRP	Standard Review Plan
SSE	Safety Shutdown Earthquake
US-APWR	United States-Advanced Pressurized Water Reactor
WPMR	Whole Pool Multi-Rack

1.0 INTRODUCTION

This report considers the structural adequacy of the proposed Spent Fuel Racks (SFR) and the New Fuel Racks (NFR) for the United States-Advanced Pressurized Water Reactor (US-APWR). The SFR are placed inside the pit whereas the NFR are placed outside the pit. All analyses and evaluations follow the US Office of Technology (OT) Position Paper (Reference 6-1) and the U.S. NRC Standard Review Plan (SRP) (Reference 6-2) whichever is more limiting. The dynamic analyses employ a time-history simulation code used by Holtec International for numerous previous licensing efforts in the US and abroad.

This report provides a discussion of the method of analyses, modeling assumptions, key evaluations, and the results obtained to establish the margins of safety.

This report establishes the structural integrity of the SFR and NFR under seismic loading. The objective of this report is to develop the loads on the fuel racks and to confirm that the loads do not pose a threat to active fuel.

The module layout for the SFR and NFR to be installed is illustrated in Figure 2-1. The SFR layout consists of Six (6) SFRs and two (2) Damaged Fuel Racks (DFR) with a combined storage capacity of 912 cells. The NFR layout consists of three (3) NFRs which provide a total storage capacity of 180 cells.

2.0 US-APWR FUEL RACKS

The SFR modules are shown in Figure 2-1. Spent fuel is stored in moderate density racks to be installed in the spent fuel pit (SFP) filled with borated water. The SFR have the capacity to store 900 fuel assemblies, and the center-to-center spacing between adjacent fuel assemblies is nominally 11.1 inch to maintain subcriticality. The cell wall thickness of the SFR is 0.090 inch.

The DFR modules are shown in Figure 2-1 along with the SFR modules. Twelve locations are included to support damaged fuel assembly container (DFAC). The DFR storage cells are square in shape and have a cell wall thickness of 0.375 inch. The DFR have a cell pitch of 24 inch. The DFAC shall be installed within the DFR in the SFP.
The DFAC shall have the capability to confine gross fuel particles, debris, etc.
The NFR modules are shown in Figure 2-1. New fuel is stored in low density racks installed in the dry new fuel pit (NFP). The NFRs store 180 fuel assemblies, and the center-to-center spacing between adjacent fuel assemblies is nominally 16.9 inch to maintain subcriticality. The cell wall thickness of the NFR is 0.209 inch.

All SFRs and NFRs are freestanding and self-supporting. The principal construction materials for the racks are SA240-304 or -304L stainless steel sheet and plate stock, and SA564-630 precipitation hardened stainless steel bar for adjustable support spindles. The only non-stainless material utilized in the rack is the neutron absorber material, which is a boron carbide and aluminum metal matrix composite available under the patented product name Metamic^{TM}.

The SFRs and NFRs have been designed to meet the stress limits of, and have been analyzed in accordance with, Section III, Division I, Subsection NF of the American Society of Mechanical Engineers (ASME) Boiler and Pressure Vessel (B&PV) Code (Reference 6-3). The structural materials of the racks will be procured in accordance with the specifications of

Section II of the ASME B&PV Code (Reference 6-4). All applicable structural welds will be performed using procedures developed and qualified in accordance with Section IX of ASME B&PV Code (Reference 6-5).

Figure 2-2 provides the isometric schematics of the SFR. Each SFR module is supported by four pedestals, which are remotely adjustable. “Top plates” are designed on each rack module which is welded just below the top of each rack elevation (surrounding the rack). The top plates on each rack are aligned at the same elevation and are designed such that there exists a 0.125 inch gap between each plate. The intension of this design is to avoid impact between rack cell walls during a seismic event and instead allow the top plates to bear the impact. The pedestals are designed to be placed over 3 inch thick “bearing pads”. In order to have the racks move in unison during an event, the bearing pads are designed to accommodate pedestals from different racks.

Figure 2-3 provide the isometric schematic of the NFR. The NFR module is supported by five or six pedestals, which are remotely adjustable. There are 5 pedestals on the 7x9 racks and 6 pedestals on the 7x8 rack. The NFR also incorporates “top plates” similar to the SFR. There are 2 two plates on each NFR separated by a distance of 9 inch. The distance between the top plates on each rack is 0.125 inch. There are “adjustable supports” that are welded to the top of the rack between the top plates. The threaded supports are extended such that there exists a gap of 0.125 inch between the storage pit wall and the supports (Reference 6-24).

The overall designs of the rack modules are similar to those presently in service in the SFPs at many other nuclear plants. Altogether, Holtec International has provided over 50 thousand storage cells of these designs to various nuclear plants around the world.

The rack modules are designed as cellular structures such that each fuel assembly has a square opening with conforming lateral support and a flat horizontal-bearing surface. All of the spent fuel storage locations are constructed with multiple cooling flow holes to ensure that redundant flow paths for the coolant are available. The basic characteristics of the fuel racks are summarized in Table 2-1 through 2-3.

3.0 STRUCTURAL/SEISMIC CONSIDERATION

3.1 Methodology

3.1.1 Acceleration Time Histories

The response of a freestanding rack module to seismic inputs is highly nonlinear and involves a complex combination of motions (sliding, rocking, twisting, and turning), resulting in impacts and frictional effects. Linear methods, such as modal analysis and response spectrum techniques, cannot accurately replicate the response of such a highly nonlinear structure to seismic excitation. An accurate simulation is obtained only by direct integration of the nonlinear equations of motion using actual pit slab acceleration time-histories as the forcing function. Therefore, initial step in US-APWR fuel racks qualification is to develop synthetic time-histories for three orthogonal directions that comply with the guidelines of the NRC SRP (Reference 6-6).

The SFRs and NFRs have been analyzed using five different sets of acceleration time histories. Five sets of 3-D acceleration-time histories are generated using the target response spectra data and the seed data. The target response spectra data corresponding to the 4% damped Safety Shutdown Earthquake (SSE) are shown in Figures 3-8 and 3-9. The response spectra data are derived from the soil-structure-interaction analysis. For consistency, the same seed motions used for the US-APWR building analysis are used to develop the fuel rack time histories.

Each set of acceleration-time histories and its corresponding response spectra are generated in accordance with USNRC requirements for time histories used as driving loads for dynamic analysis. The five sets of acceleration-time histories are shown to meet the applicable requirements for multiple time histories, as specified in the NRC SRP (Reference 6-6).

Each set of acceleration-time histories includes three mutually orthogonal components, two horizontal and one vertical. The following are the steps involved in the development of the modified real recorded time histories:

1. Obtain the design basis response spectra for all three directions, corresponding to the elevations where the racks will be deployed.

2. The five sets of real recorded ground motions, previously used for the USAPWR building analysis are input into EZ-FRISK™ as seeds for spectral matching.
   1. Chi-Chi, Taiwan @ Station ILA067, 1999
   2. Darfield @ Station DFHS, 2010
   3. Hector Mine @ Station Amboy, 1999
   4. Nahanni @ Site 3, 1985
   5. Northridge @ Mt. Baldy Elementary School, 1994

3. Using the RspMatch99 technique within EZ-FRISK™, the seed motions are scaled and matched to the target response spectra in all three directions. The response spectra and final acceleration-time histories are retrieved from EZ-FRISK™ and reviewed for SRP 3.7.1 (Reference 6-6) compliance.

The generated time histories used for seismic analysis of NFR and SFR are shown in Figures 3-10, 3-12, 3-14, 3-16, 3-18, and 3-20. For the N-S, E-W, and vertical directions, respectively. Figures 3-11, 3-13, 3-15, 3-17, 3-19, and 3-21 show the comparison between the target response spectrum and the computed average response spectrum for the five time histories for the North-South, East-West, and vertical direction for SFR and NFR, respectively.

All five ground motions selected as seed motions have time increments of 0.005 seconds and total durations exceeding 20 seconds.
The results of the correlation calculation for each of the modified acceleration-time histories are less than 0.16 indicating the desired statistical independence in all three directions. The cumulative strong motion durations calculated for each modified time history set are greater than 6 seconds.
The average of the generated response spectra are shown to envelope the corresponding target spectra, meeting the intent of SRP 3.7.1 (Reference 6-6).
The generated seismic accelerograms are suitable to simulate the seismic event for the SFR and NFR dynamic analysis. All governing criteria for development of modified real acceleration-time histories for use in seismic analysis involving non-linear system behavior are considered to be satisfied.

3.1.2 Modeling Methodology

3.1.2.1 General Considerations

Once an admissible set of input excitations is obtained, the next step in the analysis process is to develop a suitable dynamic model. Reliable assessment of the stress field and kinematic behavior of the rack modules calls for a conservative dynamic model incorporating all key attributes of the actual structure. This means that the dynamic model must have the ability to execute concurrent sliding, rocking, bending, twisting and other motion forms compatible with the freestanding installation of the modules. Furthermore, the model must possess the capability to effect momentum transfers which occur due to rattling of fuel assemblies inside storage cells and the capability to simulate lift-off and subsequent impact of support pedestals with the pit liner (or bearing pad). The contribution of the water mass in the interstitial spaces around the rack modules and within the storage cells must be modeled in an accurate manner. The Coulomb friction coefficient at the pedestal-to-pit liner (or bearing pad) interface may lie in a rather wide range and a conservative value of friction cannot be prescribed a priori.

The three-dimensional (3-D) dynamic models of a single spent fuel rack introduced by Holtec International in 1980 have been used in many re-rack projects since that time. The details of this classical methodology are published in the permanent literature (Reference 6-7). Briefly, the 3-D model of a typical rack in the SFP handles the array of variables as follows:

(1) Interface Coefficient of Friction

Coefficient of friction (COF) values are assigned at each interface, which reflect the realities of stainless steel-to-stainless steel contact. The mean value of COF is 0.5, and the limiting values are based on experimental data, which are bounded by the values 0.2 and 0.8 (Reference 6-8).

(2) Impact Phenomena

Compression-only spring elements, with gap capability, are used to provide for opening and closing of interfaces such as the pedestal-to-bearing pad interface, the fuel assembly-to-cell wall interface, and rack-to-rack and rack-to-pit wall potential contact locations.

(3) Fuel Loading Scenarios

The dynamic analyses performed for the SFRs and NFRs conservatively assume that all fuel assemblies within the rack rattle in unison throughout the seismic event, which obviously exaggerates the contribution of impact against the cell wall.

(4) Fluid Coupling

Holtec International extended Fritz's classical two-body fluid coupling model (Reference 6-9) to multiple bodies and utilized it to perform the first two-dimensional multi-rack analysis. Subsequently, laboratory experiments were conducted to validate the multi-rack fluid coupling theory. This technology is incorporated in the Whole Pool Multi-Rack (WPMR) analysis, which permits simultaneous simulation of all racks in the pit. This treatment of in-pit hydrodynamics has been used in many Holtec re-rack submittals since 1988. In its simplest form the so-called "fluid coupling effect" (References 6-9 and 6-10) can be explained by considering the proximate motion of two bodies under water. If one body (mass m_1) vibrates adjacent to a second body (mass m_2), and both bodies are submerged in frictionless fluid, then Newton's equations of motion for the two bodies are:

$$(m_1 + M_{11})\, A_1 + M_{12}\, A_2 = \text{applied forces on mass } m_1 + O(X_1^2)$$
$$M_{21}\, A_1 + (m_2 + M_{22}) A_2 = \text{applied forces on mass } m_2 + O(X_2^2)$$

A_1, A_2 denote absolute accelerations of masses m_1 and m_2, respectively, and the notation $O(X^2)$ denotes nonlinear terms. The fluid adds mass to the body (M_{11} to mass m_1), and an inertial force proportional to acceleration of the adjacent body (mass m_2). Thus, acceleration of one body affects the force field on another. This force field is a function of inter-body gap, reaching large values for small gaps. Lateral motion of a fuel assembly inside a storage location is subject to this effect. The fluid coupling, in general, is always present when a series of closely spaced bodies (fuel racks) undergo transient motion in a submerged SFP. The fluid coupling effect encompasses interaction between every set of racks in the pit (i.e., the motion of one rack produces fluid forces on all other racks and on the pit walls). Stated more formally, both near-field and far-field fluid coupling effects are included in the analysis. During the seismic event, all racks in the pit are subject to the input excitation simultaneously. The motion of each freestanding module is autonomous and independent of others as long as they do not impact each other and no water is present in the pit. As noted in References 6-9 and 6-10, the fluid forces can reach rather large values in closely spaced geometries. It is, therefore, essential that the contribution of the fluid forces be included in a comprehensive manner. This is possible only if all racks in the pit are allowed to execute 3-D motion in the mathematical model. For this reason, single rack or even multi-rack models involving only a portion of the freestanding racks in the pit, are inherently inaccurate. The fluid coupling effects between all

freestanding racks must be included in the model to properly account for the interaction of the hydrodynamic forces with the inertia and friction forces. The WPMR model removes this intrinsic limitation of the rack dynamic models by simulating the 3-D motion of all modules simultaneously. The derivation of the fluid coupling matrix relies on the classical inviscid fluid mechanics principles, namely the principle of continuity and Kelvin's recirculation theorem. The derivation of the fluid coupling matrix is not based on an artificial construct, but it has been nevertheless verified by an extensive set of shake table experiments (Reference 6-10).

3.1.2.2 Specific Modeling Details for Rack

The “building block” for the WPMR analysis is a 3-D multi-degree of freedom model for each single SFR. For the purposes of the WPMR dynamic analysis, each rack, plus contained rattling fuel, is modeled as a 22 degree of freedom (DOF) system. The rack cellular structure elasticity is modeled by a 3-D beam having 12 DOF (3 translation and 3 rotational DOF at each end so that 2-plane bending, tension/compression, and twist of the rack are accommodated). An additional two (2) horizontal DOFs are ascribed to each of five rattling fuel masses which are located at heights 0H, 0.25H, 0.5H, 0.75H and H, where H is the height of a storage cell above the baseplate. While the horizontal motion of the rattling fuel mass is associated with five separate masses, the totality of the fuel mass is associated with the vertical motion and it is assumed that there is no fuel rattling in the vertical direction. In other words, the vertical displacement of the fuel is coupled with the vertical displacement of the rack (i.e., DOF “P3” in Figure 3-1) by lumping the entire stored fuel mass (in the vertical direction only) with the vertical rack mass at the baseplate level.

The beam model for the rack is assumed supported, at the base level, on four pedestals modeled with non-linear elements; these elements are properly located with respect to the centerline of the rack beam, and allow for arbitrary rocking and sliding motions. The horizontal rattling fuel masses transfer load to the SFR through compression only gap spring elements oriented to allow impacts of each of the five rattling fuel masses with the rack cell in either or both horizontal directions at any instant in time. Figure 3-1 illustrates the typical dynamic rack model with the degrees of freedom shown for both rack and for rattling fuel. In order to simulate this behavior, the stored fuel mass is distributed among the five lumped mass nodes, for all racks, as follows:

(1) Top of rack (node 2* in Figure 3-1)	12.5% of total stored fuel mass
(2) 3/4 height (node 3* in Figure 3-1)	25% of total stored fuel mass
(3) 1/2 height (node 4* in Figure 3-1)	25% of total stored fuel mass
(4) 1/4 height (node 5* in Figure 3-1)	25% of total stored fuel mass
(5) Bottom of rack (node 1* in Figure 3-1)	12.5% of total stored fuel mass

The stiffness of pedestal springs that simulate rack pedestal to the floor compression-only contact is modeled using contact and friction elements at the locations of the pedestals between pedestal and floor. A total of four contact springs (one at each pedestal location) and 8 friction elements (two per pedestal) are included in each 22 DOF rack model.

Also shown in Figure 3-1 is a model detail of a typical support with a vertical compression only gap element and two orthogonal elements modeling frictional behavior. These friction elements resist lateral loads, at each instant in time, up to a limiting value set by the current value of the normal force times the COF. Figures 3-2 through 3-4 show schematics of the various (linear and non-linear) elements that are used in the dynamic model of a typical SFR. Specifically, Figure 3-2 shows the location of the compression-only gap elements that are used to simulate the potential for rack-to-rack or rack-to-wall contact at every instant in time. Figure 3-3 shows the four compression only gap elements at each rattling mass location, which serve to simulate rack to fuel assembly impact in any orientation at each instant in time. Figure 3-4 shows a two-dimensional elevation schematic depicting the five fuel masses and their associated gap/impact elements, the typical pedestal friction and gap impact elements. This figure combines many of the features shown in Figures 3-2 and 3-3, and it provides an overall illustration of the dynamic model used for the US-APWR fuel racks.

Finally, Figure 3-5 provides a schematic of the coordinates and the beam springs used to simulate the elastic bending behavior of the rack cellular structure in two-plane bending. Not shown are the linear springs modeling the extension, compression and twisting behavior of the cellular structure.

Mass Matrix

In addition to the structural mass, the following hydrodynamic effects of the SFP water are included in the total mass matrix:

(1) Rack-to-fuel hydrodynamic mass due to fluid motion inside each of the SFR cells.

(2) Hydrodynamic mass due to fluid movement around the SFRs in the interstitial spaces between modules.

(3) Hydrodynamic mass effects under the baseplate of each SFR.

(4) There is no water in the NFP. Therefore, the above hydrodynamic effects do not apply to the NFRs.

Stiffness Matrix

The spring stiffnesses associated with the elastic elements that model the behavior of the assemblage of cells within a rack are based on the representation developed in (Reference 6-11). Tension-compression behavior and twisting behavior are each modeled by a single spring with linear or angular extension involving the appropriate coordinates at each end of the rack beam model. For simulation of the beam bending stiffness, a model is used consistent with the techniques of the reference based on a bending spring and a shear spring for each plane of bending, which connects the degrees of freedom associated with beam bending at each end of the rack. Impact and friction behavior is included using the piecewise linear formulations similarly taken from the reference.

The SFR and NFR are subject to the SSE earthquakes described in Section 3.1.1. Ten runs have been performed (five each for the SFR and NFR) using a random value of COF, with an upper and lower bound limits of 0.8 and 0.2 respectively.

3.1.3 Simulation and Solution Methodology

The WPMR analysis process is the vehicle available for displacement and load analysis of each rack in the pit and also serves to establish the presence or absence of specific rack-to-rack or rack-to-wall impacts during the seismic event. Recognizing that the analytical work effort must deal with stress and displacement criteria, the sequence of model development and analysis steps that are undertaken for each simulation are summarized in the following:

(1) Prepare 3-D dynamic models of the assemblage of all rack modules in the pit. Include all fluid coupling interactions and mechanical couplings appropriate to performing an accurate non-linear simulation.

(2) Perform non-linear WPMR dynamic analyses for the assemblage of racks in the pit. Archive for post-processing appropriate displacement and load outputs from the dynamic model.

(3) Perform stress analysis of high stress areas for rack dynamic runs. Demonstrate compliance with ASME Code Section III, Subsection NF (Reference 6-3) limits on stress and displacement. The high stress areas are associated with the pedestal-to-baseplate connection. In addition, some local evaluations are performed for the bounding case to ensure that the fuel remains protected under all impact loads.

For the transient analyses performed in part (2) above, a step-by-step solution in time, employing a central difference algorithm is used to obtain a solution. The WPMR simulation model serves as the foundation for the analyses performed herein. The solver computer algorithm, implemented in the Holtec Proprietary Code MR216 (a.k.a. DYNARACK), is given in (Reference 6-11) and the documentation of MR216 is presented in (Reference 6-12).

Using the 22-DOF structural model for every rack that comprises a WPMR simulation, equations of motion corresponding to each DOF are obtained using Lagrange's formulation of the dynamic equations of motion (Reference 6-11). The system kinetic energy includes contributions from the structural masses defined by the 22-DOF model. The final system of equations has the matrix form:

$$[M] \{d^2q/dt^2\} = \{Q\} + \{G\}$$

where:

[M] - total mass matrix (includes structural mass contribution). The size of this matrix will be (22 x NOR) x (22 x NOR). NOR = number of racks in the SFP or NFP.

{q} - the nodal displacement vector relative to the pit slab displacement

{G} - a vector dependent on the given ground acceleration

{Q} - a vector dependent on the spring forces (linear and nonlinear) and the coupling between degrees-of-freedom

The above column vectors have length (22 x NOR).

The equations can be rewritten as follows:

$$\{d^2q/dt^2\} = [M]^{-1} \{Q\} + [M]^{-1} \{G\}$$

This equation set is mass uncoupled, displacement coupled at each instant in time. The numerical solution uses a central difference scheme built into the proprietary computer program.

Results are archived at appropriate time intervals for permanent record and for subsequent post- processing for structural integrity evaluations as follows:

(1) All generalized nodal displacement coordinate values in order to later determine the motion of the rack.

(2) All load values for linear springs representing beam elasticity.

(3) All load values for compression-only gap springs representing pedestals, rack-to-fuel impact, rack-to-rack and rack-to-wall impacts.

(4) All load values for friction springs at the pedestal/bearing pad interface.

3.1.4 Conservatisms Inherent in the Methodology

The following items are built-in conservatisms:

(1) Spring rates are computed in a conservative manner to employ maximum values in the analysis. This tends to conservatively overestimate peak impact forces.

(2) All stored fuel assemblies are conservatively assumed to rattle in unison, which exaggerates the impact momentum between the fuel and the rack.

3.2 Kinematic and Stress Acceptance Criteria

3.2.1 Introduction

The SFR and NFR are designed as seismic Category I. The OT Position Paper (Reference 6-1) and the USNRC SRP 3.8.4 (Reference 6-2) state that the ASME Code Section III, Subsection NF (Reference 6-3), as applicable for Class 3 Components, is an appropriate vehicle for design. In the following sections, the ASME limits are set down first, followed by any modifications by project specification, where applicable.

3.2.2 Kinematic Criteria

The SFR and NFR should not exhibit rotations sufficient to cause the rack to overturn (i.e., ensure that the rack does not slide off the bearing pads or exhibit a rotation sufficient to bring the center of mass over the corner pedestal).

3.2.3 Stress Limits Criteria

For thoroughness, the SRP load combinations are used. Stress limits must not be exceeded under the required load combinations. The loading combinations shown in Table 3-1 are applicable for freestanding racks that are made of steel.

Note that there is no Operating Basis Earthquake (OBE) event for US-APWR; therefore, loading conditions associated with an OBE event are not considered.

3.2.4 Stress Limits for Various Conditions Per ASME

Stress limits for Normal Conditions are derived from the ASME Code, Section III, Subsection NF. Parameters and terminology are in accordance with the ASME Code. The SFR and NFR are freestanding; thus, there is minimal or no restraint against free thermal expansion at the base of the rack. Moreover, thermal stresses are secondary which, strictly speaking, have no stipulated stress limits in Class 3 structures or components. Thermal loads applied to the rack are, therefore, not included in the stress combinations.

Material properties for analysis and stress evaluation are provided in Section 3.4.3.

3.2.4.1 Normal Conditions (Level A)

(1) Tension

Allowable stress in tension on a net section is

$$F_t = 0.6\ S_y$$

where S_y is the material yield strength at temperature. (F_t is equivalent to primary membrane stress.)

(2) Shear

Allowable stress in shear on a net section is

$$F_v = 0.4\ S_y$$

(3) Compression

Allowable stress in compression on a net section of Austenitic material is

$$F_a = S_y (0.47 - kl/444r)$$

where kl/r < 120 for all sections and

l = unsupported length of component.

k = length coefficient which gives influence of boundary conditions, e.g.

k = 1 (simple support both ends)

k = 2 (cantilever beam)

k = 0.5 (clamped at both ends)

Note: Evaluations conservatively use k=2 for all conditions

E = Young's modulus

r = radius of gyration of component = c/2.45 for a thin wall box section of mean side width c.

(4) Bending

Allowable bending stress at the outermost fiber of a net section due to flexure about one plane of symmetry is

$$F_b = 0.6\, S_y$$

(5) Combined Bending and Compression

Combined bending and compression on a net section satisfies

$$f_a/F_a + C_{mx} f_{bx}/D_x F_{bx} + C_{my} f_{by}/D_y F_{by} < 1.0$$

where:

f_a = Direct compressive stress in the section

f_{bx} = Maximum bending stress for bending about x-axis

f_{by} = Maximum bending stress for bending about y-axis

C_{mx} = 0.85

C_{my} = 0.85

$$D_x = 1 - (f_a/F'_{ex})$$

$$D_y = 1 - (f_a/F'_{ey})$$

$$F'_{ex,ey} = (\pi^2 E)/(2.15\,(kl/r)_{x,y}{}^2)$$

and subscripts x and y reflect the particular bending plane.

(6) Combined Flexure and Axial Loads

Combined flexure and tension/compression on a net section satisfies

$$(f_a/0.6\,S_y) + (f_{bx}/F_{bx}) + (f_{by}/F_{by}) < 1.0$$

(7) Welds

Allowable maximum shear stress on the net section of a weld is

$$F_w = 0.3\,S_u$$

where S_u is the material ultimate strength at temperature. For the area in contact with the base metal, the shear stress on the gross section is limited to $0.4\,S_y$.

3.2.4.2 Upset Conditions (Level B)

Although the ASME Code allows an increase in allowables above those appropriate for normal conditions, any evaluations performed herein conservatively use the normal condition allowables.

3.2.4.3 Faulted (Abnormal) Conditions (Level D)

Section F-1334 (ASME Section III, Appendix F (Reference 6-13)), states that limits for the Level D condition are the smaller of 2 or $1.167\,S_u/S_y$ times the corresponding limits for the Level A condition if $S_u > 1.2\,S_y$, or 1.4 if $S_u \leq 1.2\,S_y$ except for requirements specifically listed below. S_u and S_y are the ultimate strength and yield strength at the specified rack design temperature. Examination of material properties for 304L stainless demonstrates that 1.2 times the yield strength is less than the ultimate strength. Since 1.167 x (66,100/21,400) = 3.60, the multiplier of 2.0 controls.

Exceptions to the above general multiplier are the following:

(1) Stresses in shear in the base metal shall not exceed the lesser of $0.72\,S_y$ or $0.42\,S_u$. In the case of the austenitic stainless material used here, $0.72S_y$ governs.

(2) Axial compression loads shall be limited to 2/3 of the calculated buckling load.

(3) Combined Axial Compression and Bending - The equations for Level A conditions shall apply except that

$$F_a = 0.667 \times \text{Buckling Load} / \text{Gross Section Area},$$

and $F_{ex,ey}$ may be increased by the factor 1.65.

(4) For welds, the Level D allowable maximum weld stress is not specified in Appendix F of the ASME Code (Reference 6-13). An appropriate limit for weld throat is conservatively set here as:

$$F_w = (0.3\ S_u) \times \text{factor}$$

Where:

Factor = (Level D shear stress limit)/(Level A shear stress limit)

$= 0.72 \times S_y / 0.4 \times S_y = 1.8$

3.2.5 Dimensionless Stress Factors

In accordance with the methodology of the ASME Code, Section NF, where both individual and combined stresses must remain below certain values, the stress results are presented in dimensionless form. Dimensionless stress factors are defined as the ratio of the actual developed stress to the specified limiting value. The limiting value of each stress factor is 1.0 based on an evaluation which uses the allowable strength appropriate to Level A or Level D loading as discussed above.

R1 = Ratio of direct tensile or compressive stress on a net section to its allowable value (note pedestals only resist compression).

R2 = Ratio of gross shear on a net section in the x-direction to its allowable value.

R3 = Ratio of maximum bending stress due to bending about the x-axis to its allowable value for the section.

R4 = Ratio of maximum bending stress due to bending about the y-axis to its allowable value for the section

R5 = Combined flexure and compression factor (as defined in Section 3.2.4.1(5) above).

R6 = Combined flexure and tension (or compression) factor (as defined in Section 3.2.4.1(6) above).

R7 = Ratio of gross shear on a net section in the y-direction to its allowable value.

At any location where stress factors are reported, the actual stress at that location may be recovered by multiplying the reported stress factor R by the allowable stress for that quantity. For example, if a reported Level A combined tension and two plane bending stress factor is R_6 = 0.85, and the allowable strength value is 0.6 S_y, then the actual combined stress at that location is Stress = R_6 x (0.6 S_y) = 0.51 Sy

3.3 Assumptions

The following assumptions are used in the analysis:

(1) Fluid damping is neglected, which is a conservative assumption since it yields larger rack displacement.

(2) Modeling the total effect of *n* individual fuel assemblies rattling inside the storage cells in a horizontal plane as one lumped mass at each of 5 levels in the fuel rack is a conservative assumption.

(3) Fluid coupling forces are calculated based on the nominal fluid gaps. The fluid gaps are not updated according to the rack displacements.

3.4 Input Data

3.4.1 Rack Data

Tables 2-1 through 2-3 contain information regarding the SFR, NFR and DFR data used in the analysis. Information is taken from the Holtec rack drawings (References 6-14, 6-15 and 6-16).

3.4.2 Structural Damping

Associated with every stiffness element is a damping element that provides 4% of critical linear viscous damping for an SSE event. This is consistent with the design basis damping value for the SFR and NFR provided in Reference 6-17, and also in accordance with Regulatory Guide 1.61 (Reference 6-18).

3.4.3 Material Data

The necessary material data are shown in Table 3-2. This information is taken from ASME Code Section II Part D (Reference 6-4). The values listed correspond to a temperature of 200^{o}F.

3.5 Computer Codes

All computer codes used in this analysis are presented in Table 3-3.

3.6 Analyses

3.6.1 Acceptance Criteria

The dimensionless stress factors, discussed in Section 3.2.5, must be less than 1.0. In addition,

(1) Cell wall stress shall be shown to remain below the critical buckling stress

(2) Weld and base metal stresses must remain below the allowable stress limits corresponding to the material and load conditions, as discussed in greater detail in following sections.

3.6.2 Dynamic Simulations

As discussed earlier, five simulations are performed for SFR and NFR. The combinations of the COFs and seismic inputs are shown in Table 3-4. The simulations consider SSE excitations and are required to satisfy the stress and kinematic criteria of References 6-1 and 6-2. A sensitivity run with the bounding time history (from the SFR results) was also performed with the mixed loading condition in which the total number of fuel assemblies on each rack varies by a certain percentage. The distribution is 25%, 66%, 33%, 100%, 0% and 50% for Racks 1, 2, 3, 4, 5 and 6 respectively. The mixed loading configuration was incorporated based on the discussions with the NRC on previous submittals. The purpose was to show a random distribution of assemblies on each rack structure and quantify the response. The distribution is shown in Figure 3-22.

The “random” coefficients of friction assigned for each SFR and NFR pedestal are provided in Tables 3-11 and 3-12.

3.7 Results of Analyses

3.7.1 Time History Simulation

The time histories are shown in Figure 3-10, 3-12, 3-14, 3-16, 3-18 and 3-20. Table 3-5 presents the results for major parameters for the SFR and NFR for each simulation.

To insure that the fuel racks have adequate safety margins, all subsequent stress evaluations for the fuel racks are based on the worst-case results from all twelve runs.

The sensitivity run for the mixed loading condition and the DFR run was performed with time history set 1 due to the fact that time history set 1 produces the maximum vertical load and the maximum shear load on a single pedestal from all runs. Additionally, time history set 1 produces the maximum displacement at the top and the baseplate location. The maximum stress factor (0.271) from time history set 1 is only 7.8% less than the maximum stress from all runs (0.294). Hence, time history set 1 is chosen as the bounding time history for the sensitivity run.

The results for the sensitivity run are provided in Table 3-5. The result for the DFR run (to evaluate the cell impact) is also provided in Table 3-5.

3.7.2 Time History Simulation Results

3.7.2.1 Rack Displacements

The post-processor results summarized in Table 3-6 provide the maximum absolute displacements at the top and bottom corners (in the E-W or N-S horizontal direction) relative to the pit slab. Since these results are very small compared to the dimensions of the rack, a large margin of safety exists against rack overturning.

The maximum vertical lift-off of a SFR from the pit floor during an earthquake is 1.15 inch. The pedestals on each rack are located on the recessed bearing pad holes (depth is 3 inch) and hence there is no real baseplate overlap concern for SFR.

Baseplate overlap is not an issue for the NFR because the NFP is dry (i.e., no water). Thus, a critical reaction cannot occur unless the NFP becomes flooded with water while an earthquake is occurring. Since this involves 2 simultaneous accident events (i.e., flood accident and earthquake), it is exempt from analysis per the double contingency principle.

3.7.2.2 Pedestal Vertical Forces

For SSE, the maximum vertical load on any SFR pedestal is 579,000 lbf and on any NFR pedestal is 299,000 lbf. These loads should be used to assess the structural integrity of the pit slab under the seismic event.

3.7.2.3 Pedestal Friction Forces

For SSE, the maximum Shear load on any SFR pedestal is 259,000 lbf and on any NFR pedestal is 142,000 lbf. These maximum results are used as an input loading to evaluate the female pedestal-to-baseplate weld (discussed in Section 3.7.3.2).

3.7.2.4 Impact Loads

The impact loads such as fuel-to-cell wall, rack-to-rack, and rack-to-wall impacts are discussed below.

(1) Fuel–to Cell Wall Impact Loads

For the SFR, a maximum fuel assembly-to-cell wall impact load (2,058 lbf) generates an impact acceleration as follows.
For the five-lumped mass model (with 25% at the 1/4 points and 12.5% at the ends), the maximum g-load that the rack impacts on the fuel assembly can be computed as:

$$a = \frac{4F}{w} = 4.31g$$

where: a = maximum lateral acceleration in g's

F = maximum fuel-to-cell wall impact force (= 2,058 lbf for SFR)

w = weight of one fuel assembly (1,912 lbf)

For the NFR, a maximum fuel assembly-to-cell wall impact load (5,477 lbf) generates an impact acceleration of

$$a = \frac{4F}{w} = 11.46g$$

For the DFR, a maximum fuel assembly-to-cell wall impact load (6,438 lbf) generates an impact acceleration of

$$a = \frac{4F}{w} = 13.47g$$

The fuel impact decelerations calculated above are less than the impact load limits established by the fuel manufacture (Reference 6-25).

(2) Rack-to-Rack and Rack-to-Wall Impacts

The summary result files from MR216 (Reference 6-12) in all of the simulations have been scanned to determine the maximum impact on each side of rack. The maximum impact loads generated at the SFR and NFR are summarized in Table 3-7. The stress evaluations about top plate, adjustable support and baseplate are performed in Reference 6-19 and these results are summarized in Table 3-9.

No rack-to-wall impacts occur on the SFR. The maximum impact load between the top plates on the SFR among all runs is 396,600 lbf. The compressive stress (assuming half the width of the top plate to take the impact) due to the maximum impact at the top plate is 5,691 psi and it is small compared to the yield strength of the plate material (21,400 psi). The weld stress between the top plate and rack cell due to the maximum impact is 17,113 psi which is within the allowable limit.

For NFR, the adjustable supports are designed to undergo impact against the wall during a seismic event. The maximum impact load between adjustable support and wall among all runs is 658,100 lbf. The thread shear stress in the adjustable support is 12,014 psi and it is within the allowable limits. The weld stress between the adjustable support and top plate is 30,266 psi and it is within the allowable limit.

The maximum impact load between the top plates on the NFR among all runs is 465,000 lbf. The compressive stress (assuming half the width of the top plate to take the impact) due to the maximum impact at the top plate is 3,875 psi and it is small compared to the yield strength of the plate material (21,400 psi). The weld stress between the top plate and rack cell due to the maximum impact is 3,963 psi which is within the allowable limit.

The maximum impact load between the baseplates on the NFR among all runs is 151,500 lbf. The compressive stress (assuming half the width of the baseplate to take the impact) due to the maximum impact at the baseplate is 2,690 psi and it is small compared to the yield strength of the plate material (21,400 psi).

3.7.3 Rack Structural Evaluation

3.7.3.1 Rack Stress Factors

With time history results available for pedestal normal and lateral interface forces, the limiting bending moment and shear force at the baseplate-to-pedestal interface may be computed as a function of time. In particular, maximum values for the previously defined stress factors can be determined for every pedestal in the SFR and NFR. Using this information, the structural integrity of the pedestal can be assessed. The net section maximum (in time) bending moments and shear forces can also be determined at the bottom of the cellular structure. Based on these, the maximum stress in the limiting rack cell (box) can be evaluated.

These locations are the most heavily loaded net sections in the structure so that satisfaction of the stress factor criteria at these locations ensures that the overall structural criteria set forth in Section 3.2 are met.

The summary of the maximum stress factors for the SFRs and NFRs are provided in Table 3-8.
The need for an adjustment factor accounting for ASME Code slenderness ratio evaluation is addressed in Reference 6-19, and the adjusted factors are identified with a note in Table 3-8. Note that the stress factors are computed conservatively using the material properties of SA240-304L.

All stress factors, as defined in Section 3.2, are less than the mandated limit of 1.0 for all racks for the governing faulted condition examined. Therefore, the rack is able to maintain its structural integrity under the worst loading conditions.

The maximum vertical load and shear load on a single pedestal for the SFRs and NFRs are given in Table 3-5.

3.7.3.2 Weld Stress

Weld locations in the SFR and NFR are subjected to significant seismic loading at the bottom of the rack at the baseplate-to-cell connection, at the top of the pedestal support at the baseplate connection, and at the cell-to-cell connections. Bounding values of resultant loads are used to qualify the connections.

(1) Baseplate-to-Rack Cell Welds

As stated in Section 3.2.4.3, the allowable weld stress for Level D is 0.54 S_u, which equals 35,694 psi.

Weld stresses are determined through the use of a simple conversion (ratio) factor (based on area ratios) applied to the corresponding stress factor in the adjacent rack material

$$\frac{0.090 \times (8.8 + 0.090)}{0.0625 \times 0.7071 \times 6.5} = 2.79 \text{ (For the SFR)}$$

where

0.090	is the cell wall thickness
8.8+0.090	is the mean box dimension
0.0625x0.7071	is the box-baseplate fillet weld throat size
6.5	is the length of the weld

For the NFR, the cell wall thickness and weld size are 0.209 inch and 0.125 inch respectively. The ratio factor for the NFR then becomes 3.28.

The highest predicted cell to baseplate weld stress is calculated based on the highest R6 value for the rack cell region tension stress factor and R2 and R7 values for the rack cell region shear stress factors (refer to Section 3.2.5 for definition of these factors). These cell wall stress factors are converted into weld stress values as follows:

For SFR, SSE Simulation

$\{[R6 \times (1.2)]^2 + [R2 \times (0.72)]^2 + [R7 \times (0.72)]^2\}^{1/2} \times S_y \times Ratio$
$= \{[0.294 \times (1.2)]^2 + [0.058x (0.72)]^2 + [0.071 \times (0.72)]^2\}^{1/2} \times (21,400) \times 2.79$
$= 21,430$ psi

For NFR, SSE Simulation

$\{[R6 \times (1.2)]^2 + [R2 \times (0.72)]^2 + [R7 \times (0.72)]^2\}^{1/2} \times S_y \times Ratio$
$= \{[0.177 \times (1.2)]^2 + [0.049 \times (0.72)]^2 + [0.032 \times (0.72)]^2\}^{1/2} \times (21,400) \times 3.28$
$= 15,199$ psi

The above calculation is conservative because the maximum stress factors used above do not all occur at the same time instant. The R6 value used in the above equation is the maximum unadjusted value that is output directly from DYNAPOST (Reference 6-20). The reason that this value is used, as opposed to the maximum adjusted value from Section 3.7.3.1, is because the conversion ratio is computed based on the full metal area of a single cell, not the effective cell area that is computed in Reference 6-19.

Table 3-9 shows that the calculated weld stresses are less than the corresponding allowable stress limit.

(2) Baseplate-to-Pedestal Welds

The rack weld between baseplate and support pedestal is checked using conservatively imposed loads in a separate finite element model. Table 3-9 summarizes the result derived in Reference 6-19 and the calculated weld stresses are less than the corresponding allowable stress limit.

(3) Cell-to-Cell-Welds

Cell-to-cell connections are by a series of connecting welds along the cell height. Stresses in storage cell to cell welds develop due to fuel assembly impacts with the cell wall. These weld stresses are conservatively calculated by assuming that fuel assemblies in adjacent cells are moving out of phase with one another so that impact loads in two adjacent cells are in opposite directions; this tends to separate the two cells from each other at the weld. Cell-to-cell weld calculations are performed in Reference 6-19 and are based on the maximum fuel-to-cell impact load from all runs. Both the weld and the base metal shear results are reported in Table 3-9 and the weld and the base material shear results are less than the corresponding allowable stress limit.

3.7.3.3 Pedestal Thread Shear Stress

Section 3.7.2.2 specifies the maximum vertical force on a pedestal. Using this value the maximum average shear stress in the engagement region is calculated in Reference 6-19.

The allowable shear stress for Level D conditions is the lesser of:0.72 S_y = 15,408 or 0.42 x S_u=27,762 psi (based on S_y and S_u for SA240-304L at 200°F). Therefore, the former criteria controls, and the limiting result is detailed in Table 3-9 and the pedestal thread shear stress is less than the corresponding allowable stress limit.

3.7.4 Dead Load Evaluation

The dead load condition is not a governing condition for either SFR or NFR fuel racks since the general level of loading is far less than the SSE load condition. To illustrate this, it is shown in Table 3-10 that the maximum pedestal load is low as compared to the peak seismic load and that further stress evaluations are unnecessary.

This load will induce very low stress levels in the neighborhood of the pedestal, compared with the load levels that exist under the SSE load condition. Since there are no primary shear loads on the pedestal and the Level A loads are approximately 16% of the Level D loads, while the Level A limits exceed 50% of the Level D limits, the SSE load condition bounds the dead load condition and no further evaluation is performed for dead load only. This evaluation bounds the NFRs as well.

3.7.5 Local Stress Considerations

(1) Cell Wall Buckling

The loading on a rack wall is shown in Figure 3-6. The allowable local buckling stress in the fuel cell walls (from vertical loading) is obtained by using classical plate buckling analysis on the lower portion of the cell walls. The following formula for the critical stress has been used.

$$\sigma_{cr} = K \frac{E}{1-\nu^2}\left(\frac{t}{b}\right)^2$$

where E = 27.6 x 10^6 psi, ν is Poison's ratio=0.3, t = 0.090" for the SFR or t=0.209” for the NFR, b = 8.8". The *K* factor varies depending on the plate length/width ratio and the boundary support conditions at the sides of the plate. At the base of the rack, the cell wall acts alone in compression for a length of about 12 inch up to the point where the poison sheathing is attached. Above this level, the sheathing provides additional strength against buckling, which is not considered here. Therefore, the length/width ratio for the 8.8 inch wide cell wall will be taken as 1.36. From Table 35 of Reference 6-21, the value of *K* is taken as 5.76, which is the corresponding value for a/b (length/width ratio) = 1.4, for two sides simply supported and two side clamped.

For the given data

σ_{cr} < 18,273 psi for the SFR

< 98,541 psi for the NFR

It is conservative to apply the above equation to the rack cell wall if we compare σ_{cr} with the maximum compressive stress anywhere in the cell wall. This local buckling stress limit is not violated anywhere in the body of the rack modules, since the maximum compressive stress in the outermost cell is:

SSE Simulation:

σ = (1.2) x (21,400) x R6 (which is 0.294) = 7,550 psi for the SFR

= (1.2) x (21,400) x R6 (which is 0.177) = 4,545 psi for the NFR

which are less than 18,273 psi or 98,541 psi. Therefore, rack cell wall buckling does not occur.

(2) Secondary Stresses Produced by Temperature Effects.

The temperature gradients across the rack structure caused by differential heating effects between one or more filled cells and one or more adjacent empty cells are considered. This secondary stress condition is evaluated alone and not combined with primary stresses from other load conditions.

A thermal gradient between cells will develop when an isolated storage location contains a fuel assembly emitting maximum postulated heat, while the surrounding locations are empty. A conservative estimate of the weld stresses along the length of an isolated hot cell is obtained by considering a beam strip uniformly heated by 75°F which is conservative, and restrained from growth along one long edge. Figure 3-7 depicts a simple model for the calculation of the thermal stress in the cell of the rack. The temperature rise easily envelops the difference between the maximum local SFP water temperature (187°F bounding) inside a storage cell and the bulk pit temperature (158.9°F) based on the thermal-hydraulic analysis of the SFP (Reference 6-22).

The strip is subjected to the following boundary conditions (Refer to Figure 3-7):

(a) Displacement Ux (x,y) = 0 at x = 0 and at y = H/2 for all x

(b) Average force Nx (x) = 0 at x = L

Using shear beam theory and subjecting the strip to a uniform temperature rise Δt = 75°F, an estimate of the maximum value of the average shear stress in the strip can be calculated. The final shear stress result for the strip is found to be

$$\tau \max = \frac{E\alpha\Delta t}{0.931}$$ (Maximum at x=L)

Where E =27.6x10^6 psi

$\alpha = 9.5\times10^{-6}$ in/in°F

Δt = 75°F

Therefore, an estimate of maximum weld shear stress in an isolated hot cell, due to thermal gradient is computed, as τ_{max}= 21,124 psi.
Since this is a secondary thermal stress, we use the allowable shear stress criteria for faulted conditions (0.42xS_u=27,762 psi) as a guide to indicate that this maximum shear is acceptable.

(3) Hydrodynamic Pressure

The hydrodynamic pressure on the SFP walls during a seismic event is calculated for the SFR and DFR in Reference 6-19. Figure 3-23 shows a plot of the hydrodynamic pressure between the SFR (or DFR) and the SFP walls around the entire perimeter for the governing time history based on the WPMR results (Set 1). The maximum pressure value is 10.5 psi.

(4) Bearing Pad Analysis

For SFR, the pedestals are designed to undergo impact (vertically and horizontally) against the bearing pad during a seismic event. The maximum vertical and horizontal impact loads between pedestal and bearing pad are 579,000 lbf and 188,000 lbf respectively. The vertical and horizontal compression stresses in the bearing pad are 5,790 psi and 6,267 psi, and they are very small compared to the yield strength of the pad material.
Bearing pad analysis is performed in Reference 6-19 and the stress evaluations are summarized in Table 3-9.

(5) Thermal Expansion of Fuel Assembly

The thermal expansion of the fuel assembly is calculated for conservative expansion based on the assumption that thermal expansion of the fuel assembly and the SUS 304 material is identical. The following equation expresses the temperature dependence of the elongation of SUS 304 steel due to thermal expansion.

$$\varepsilon = 1.57\times10^{-5} \times ((T-32) \times 5/9+273.15) + 1.69\times10^{-9} \times ((T-32) \times 5/9+273.15)^2$$

(application range: $80 \leq T \leq 2548$ °F ($27 \leq T \leq 1398$ °C))

ε: Thermal expansion elongation of SUS 304 steel (in/in)
T: Temperature (°F) = 209 °F [bounding peak local fuel cladding temperature from Reference 6-22]

Using the bounding peak local fuel cladding temp (209 °F), the thermal expansion is calculated to be 0.006 (in/in). The calculated expansion value is very small and is considered to have a negligible effect on the overall analysis. Therefore, a WPMR run is not warranted to address the thermal expansion issue.

4.0 MECHANICAL ACCIDENTS

This section provides information on the required mechanical accident performance characteristic of the US-APWR fuel racks.

4.1 Description of Mechanical Accidents and Acceptance Criteria

The US NRC OT position paper (Reference 6-1) specifies that the design of the racks must ensure the functional integrity of the fuel racks under all credible fuel assembly drop events. Four categories of mechanical accidents are considered. Each of these four categories is described in the following paragraphs.

(1) Straight shallow drop event (Figure 4-1)

In the so-called “straight shallow drop” event, an impactor (i.e., a fuel assembly plus its handling tool) is assumed to drop vertically and hit the top of the rack. Inasmuch as the racks are of honeycomb construction, the deformation produced by the impact is expected to be confined to the cell walls that are directly impacted. The acceptance criterion for the “straight shallow drop” event is that the fuel storage array remains subcritical. The rack cell wall plastic deformation is not allowed to extend down into the active fuel region to undermine the criticality performance of the rack. However, for conservatism, the acceptance criteria is assumed to be the minimum distance (considering the tolerances) between the top of the rack and the upper boundary of the “neutron absorber zone” such that the acceptance criteria is 11.162 inch. The “neutron absorber zone” is the region where the neutron absorber attaches to the rack cell. To conservatively estimate the cell wall plastic deformation, the rack is assumed to absorb the maximum kinetic energy generated by the impactor.

(2) Straight deep drop event

The so-called “straight deep drop” event postulates that the impactor falls through an empty storage cell impacting the rack baseplate.
The deep drop event can be classified into two scenarios (i.e., the second and the third types of accidents), namely, drop in an interior cell away from the support pedestals (Figure 4-2), and drop through the cell located above a support pedestal (Figure 4-3).

(a) Deep drop scenario 1 (Figure 4-2)

In deep drop scenario 1, the impactor strikes the rack baseplate away from the support pedestal, where it is more flexible. If the baseplate is pierced by the fuel assembly or deforms sufficiently, the liner may be damaged leading to an uncontrollable loss of water. An additional consideration is that the baseplate deformation may lead to an abnormal condition, where the fuel assembly active zone is outside the neutron absorber-equipped space of the fuel rack. This condition must be considered in the criticality evaluations and must be limited to ensure criticality control. Severing and large deflection of the baseplate leading to a secondary impact with the pit liner are unacceptable results.

(b) Deep drop scenario 2 (Figure 4-3)

In deep drop scenario 2, the rack baseplate is buttressed by the support pedestals and presents a hardened impact surface, resulting in a high impact load. The principal design objective is to ensure that the support pedestal does not tear the liner that overlays the reinforced concrete pit slab.

(3) Stuck fuel event

In addition to the preceding drop accidents, a fourth “stuck fuel” accident is analyzed to determine the damage to the rack due to a 4,400 lbf uplift force applied to the rack by a stuck fuel assembly. Similar to the shallow drop accident, the damage to the cell wall shall be limited to the portion of the rack structure above the neutron absorber.

Normally, new fuel assemblies are stored in racks in a dry condition and the drop accidents alone have no reactivity consequence. Therefore, the shallow drop accident for NFR is not required.

The following observations indicate that the SFR is weaker than the NFR in construction. Therefore, the drop accidents for NFR are bounded by the drop accidents for SFR.

1) The thickness of material used in the construction of the NFR cells is 0.209 inch, which is more than two times thicker than the material used for SFR cells (0.090 inch).

2) The NFR observes lower normal and accident temperatures than the SFR and hence sets higher allowable limits for the NFR material.

3) The weight of the dropped spent fuel is heavier (2,450 lbf) than the new fuel (2,000 lb).

Only the SFR are evaluated for all the plausible accident conditions in the succeeding sections.

4.2 Analysis Methods

The finite element method is used to carry out the impact analysis for the postulated drop accidents. LS-DYNA, a commercial computer code developed by the Livermore Software Technology Corporation and independently validated by Holtec International through its quality assurance (QA) program, is used to numerically simulate the impact events. This analysis methodology has been applied to drop analyses for numerous Holtec wet storage projects accepted by the USNRC.

The subsections that follow describe the analysis methods to be used in performing licensing-basis calculations to demonstrate that the mechanical accident performance requirements for the fuel racks are satisfied. These are intended to be minimum requirements, and more sophisticated analysis models may be used. Similar mechanical accident analyses have been used for previous fuel rack licensing at many nuclear plants worldwide by Holtec International.

In accordance with the OT position paper (Reference 6-1), this report performs a total of 3 drop analyses/calculations that cover all possible drop scenarios for all US-APWR racks. The 3 drop events are identified in Table 4-1.

4.2.1 Calculation of Incident Impact Velocity

A dropped fuel assembly is modeled as a single lumped mass under the influence of gravity in a drag inducing medium. The effects of virtual mass, gravity, and fluid drag are accounted for in the model. The virtual mass is assumed equal to the buoyant mass of the fuel assembly. The drag force is based on the exposed frontal area of the fuel assembly. The governing equation for a body of mass subject to gravity and drag effects is:

$$(M + M_v)\frac{d^2x}{dt_2} + \frac{C_D}{2} d_w A_D \left(\frac{dx}{dt}\right)^2 = (M - M_v)g$$

where:

M = Dry mass of the impactor

M_v = Virtual mass of the impactor (Buoyant mass)

C_D = Effective drag coefficient due to all contributing effect

d_w = Mass density of the water

A_D = Area subject to drag forces

v = Velocity of the object

g = Gravitational acceleration

x = Distance

t = Time

For a drop from a given height, the initial conditions are:

$$t = 0, x = 0, \frac{dx}{dt} = 0$$

The above nonlinear second order differential equation is readily solved to obtain the incident impact velocity.

4.3 Analysis Results

In the first step of the solution process, the velocity of the dropped object (impactor) is computed for the condition of underwater free fall in the manner of the formulation presented in the section above. Table 4-1 contains the drop height, impactor weight and computed velocities for the various drop events.

In the second step of the solution, an elasto-plastic finite element model for each drop event is prepared with the Holtec QA validated computer Code LS-DYNA. The model simulates the transient collision event with full consideration of plastic, large deformation, wave propagation, and elastic/plastic buckling modes. Table 4-2 lists the material properties of the rack structural members.

In the “shallow” and the “deep” drop events, the fuel assembly is modeled by an equivalent elasto-plastic rod with a concentrated mass (representing the handling tool) and a properly modeled rigid end-fitting at its two extremities. The structurally weakest impact region is considered in performing the “shallow” and the “deep” drop analysis. Shell elements are used to model the thin cell walls and weld connections. The rack baseplate is modeled with thick shell elements. Moreover, the rack support female block and pedestal are modeled with solid elements. The dropped fuel assembly end fittings are conservatively assumed rigid in all drop events, thereby eliminating any energy loss in these components during a postulated drop event. The fuel cladding is modeled using beam elements with elastic material properties for conservatism.

The detailed calculations are contained in Reference 6-23 for the drop accident analyses, and Reference 6-19 for the stuck fuel analyses.

4.3.1 Straight Shallow Drop Event

Figure 4-4 shows the maximum plastic deformation of the rack resulting from the shallow drop event. It can be seen that the plastic deformation of the cell wall due to a shallow drop event is 10.371 inch, which is below the acceptance criterion of 11.162 inch. This plastic deformation is limited to the region above the “neutron absorber zone” and therefore the postulated shallow drop event will result in acceptable consequences.

4.3.2 Straight Deep Drop Events

Figure 4-5 shows the peak baseplate vertical deformation of deep drop scenario 1. The fuel assembly support surface is lowered by a maximum of 1.851 inch, which is less than the distance of 11.75 inch from the baseplate to the liner. The pool liner will not be contacted by the deformed baseplate. Therefore, the deep drop scenario 1 produced some deformation of the baseplate, but the baseplate was not pierced.

In the deep drop scenario 2, the impact force between the pool floor and rack pedestal is 227,240 lbs which is less than the vertical pedestal load (579,000 lbf) from rack seismic analysis as described in Section 3.7 of this report. Therefore, this accident case is bounded by the rack seismic analysis of the racks.

4.3.3 Stuck Fuel Event

Result of the analysis show that the maximum stresses for SFR and NFR due to a stuck fuel assembly are only 1,389 psi and 598 psi respectively, which are well below the material yield stress. Therefore, the fuel racks are adequate to withstand a 4,400 lbf uplift force due to a stuck fuel assembly.

4.4 Conclusions of Mechanical Analysis

As mentioned above, the NFR damages from mechanical accidents are bounded by the SFR damages from mechanical accidents. Several mechanical accidents for SFR and NFR have been analyzed and found to produce localized damage well within the design limits for the racks.

The straight shallow drop event produces some localized plastic deformation in the top of the storage cell, but the region of permanent strain is limited to the portion of the rack structure above the “neutron absorber zone”.

The analysis of deep drop scenario 1 at cell locations selected to maximize baseplate deformation indicates that the baseplate will not experience puncture and the downward displacement of the baseplate will not lead to a secondary impact of the fuel assembly with the pit liner.

The analysis of deep drop scenario 2 shows that the rack and the pedestal remain structurally adequate.

Finally, the stuck fuel event analysis indicated that no damage to the cell wall occurs.

5.0 CONCLUSIONS

From the results of the WPMR and mechanical accident analyses, the following conclusions are made regarding the new design and layout of the SFR, DFR and NFR for the US-APWR:

(1) All rack cell wall and pedestal stress factors are below the allowable stress factor limit of 1.0.

(2) There are no rack-to-wall impacts involving the SFR and DFR. Adjustable supports which are welded between the two top plates of the NFR have impacts against the wall and the resultant loads are shown to be well within the allowable limits.

(3) All weld stresses are below the allowable limits.

(4) The NFR do experience rack-to-rack impacts during SSE events at the baseplate because they are in contact by design. However, the impact loads are much lower than the allowable limit of the baseplate.

(5) The SFR and NFR do experience rack-to-rack impacts during SSE events at the top plate because they are in contact by design. However, the impact loads are much lower than the allowable limit of the top plate.

(6) A stuck fuel assembly does not cause a bounding stress condition.

(7) The fuel racks possess acceptable margins of safety under the postulated mechanical accidents.

It is therefore considered demonstrated that the design of the SFR, DFR and NFR meets the requirements for structural integrity for the postulated Level A and Level D conditions defined.

6.0 REFERENCES

6-1 USNRC Office of Technology Position for Review and Acceptance of Spent Fuel Storage and Handling Applications, dated April 14, 1978, and January 18, 1979 amendment.

6-2 Other Seismic Category I Structures, Standard Review Plan for Safety Analysis Reports for Nuclear Power Plants, NUREG-0800, Standard Review Plan Section 3.8.4, Rev.2, U.S. Nuclear Regulatory Commission, Washington, DC, March 2007.

6-3 Supports, Rules for Construction of Nuclear Facility Components, American Society of Mechanical Engineers (ASME) Boiler & Pressure Vessel Code Section III, Division 1, Subsection NF, 2001 Edition through the 2003 Addenda.

6-4 Properties (Customary) Materials, American Society of Mechanical Engineers (ASME) Boiler & Pressure Vessel Code Section II, Part D, 2001 Edition through the 2003 Addenda.

6-5 Welding and Brazing Procedures, Welders, Brazers, and Welding and Brazing Operations, American Society of Mechanical Engineers (ASME) Boiler & Pressure Vessel Code Section IX, 2001 Edition through the 2003 Addenda.

6-6 Seismic Design Parameters, Standard Review Plan for Safety Analysis Reports for Nuclear Power Plants, NUREG-0800, Standard Review Plan Section 3.7.1, Revision 3, U.S. Nuclear Regulatory Commission, Washington, DC, March 2007.

6-7 Soler, A.I. and Singh, K.P., Seismic Responses of Free Standing Fuel Rack Constructions to 3-D Motions, Nuclear Engineering and Design, Vol. 80, pp. 315-329 (1984).

6-8 Rabinowicz, E., Friction Coefficients of Water Lubricated Stainless Steels for a Spent Fuel Rack Facility," MIT, a report for Boston Edison Company, 1976.

6-9 Fritz, R.J., The Effects of Liquids on the Dynamic Motions of Immersed Solids, Journal of Engineering for Industry, Trans. of the ASME, February 1972, pp. 167-172.

6-10 Paul, B., Fluid Coupling in Fuel Racks: Correlation of Theory and Experiment, (Proprietary), NUSCO/Holtec Report HI-88243.

6-11 Levy, S., and Wilkinson, John, The Component Element Method in Dynamics, McGraw Hill, 1976.

6-12 Holtec Computer Code MR216 (multi-rack transient analysis code, a.k.a. DYNARACK), Holtec International, New Jersey. (Holtec Proprietary)

6-13 Rules for Construction of Nuclear Facility Components, American Society of Mechanical Engineers (ASME) Boiler & Pressure Vessel Code Section III, Division 1, Appendices, 2001 Edition through the 2003 Addenda.

6-14 Outline Drawing General Arrangement, Spent Fuel Rack Design, Holtec Drawing 6174 Revision 12, Holtec International, New Jersey, February 2014. (Holtec Proprietary)

6-15 Outline Drawing General Arrangement, New Fuel Rack design, Holtec Drawing 6261 Revision 9, Holtec International, New Jersey, February 2014. (Holtec Proprietary)

6-16 Comanche Peak Damaged Fuel Container Rack Design, Holtec Drawing No. 6260 Revision 5, Holtec International, New Jersey, July 2013. (Holtec Proprietary)

6-17 US-APWR Standard Design, Design Specification of Fuel Storage Racks, N0-EH30301 Revision 11, Mitsubishi Heavy Industries, LTD. ,Tokyo Japan, August 2013.

6-18 Damping Values for Seismic Design of Nuclear Power Plants. Regulatory Guide 1.61, Revision 1, U.S. Nuclear Regulatory Commission, Washington, DC, March 2007.

6-19 Structural/Seismic Analysis for US-APWR Spent and New Fuel Storage Racks, Holtec Report HI-2084230 Revision 6, Holtec International , New Jersey, March 2014. (Holtec Proprietary)

6-20 Holtec Computer Code DYNAPOST (Analysis Post Processor), v. 2.0. , Holtec International, New Jersey. (Holtec Proprietary)

6-21 Warren C Young, Roark's Formulas for Stress & Strain, 6th edition, McGraw Hill.

6-22 Fuel Storage Racks Thermal-Hydraulic Design Package for Comanche Peck US-APWR, Holtec Report HI-2094315 Revision 5, Holtec International, New Jersey, January 2014. (Holtec Proprietary)

6-23 Mechanical Accident Analysis for Comanche Peak US-APWR Fuel Storage Racks, Holtec Report HI-2084212 Revision 9, Holtec International, New Jersey, February 2014. (Holtec Proprietary)

6-24 Spent Fuel Pool, New Fuel, & Containment Storage Rack Layout, Holtec Drawing 6173 Revision 10, Holtec International, New Jersey, February 2014. (Holtec Proprietary)

6-25 Chun, R., Witte, M. and Schwartz, M., "Dynamic Impact Effects on Spent Fuel Assemblies," UCID-21246, Lawrence Livermore National Laboratory, October 1987.

Table 2-1 Spent Fuel Rack Data*

1	Storage Cell Center-to-Center Pitch	11.1”
2	Storage Cell Inner Dimension (Width)	8.8”
3	Inter-Cell Flux Trap Gap	1.836”
4	Storage Cell Length	196”
5	Storage Cell Wall Thickness	0.090”
6	Neutron Absorber Material	METAMIC™
7	Neutron Absorber Length	( )
8	Neutron Absorber Width	( )
9	Neutron Absorber Thickness	0.106 “
10	Distance from Top of Rack Baseplate to Bottom of Neutron Absorber	11.4”
11	Neutron Absorber Sheathing Thickness	
	Internal Wall	0.024”
	Periphery Wall	0.075”
12	Baseplate Thickness	1”
13	Baseplate Flow Hole Diameter	5.5”
14	Rack Pedestal Type (Fixed or Adjustable)	Adjustable
15	Rack Pedestal Height (Female + Male)	( )
16	Rack Female Pedestal Dimensions	20” x 20” x 5”
17	Rack Male Pedestal Diameter	7”
18	Top Plate Thickness	1”

* All of the dimensions are nominal values.

Table 2-2 New Fuel Rack Data*

1	Storage Cell Center-to-Center Pitch	16.9”
2	Storage Cell Inner Dimension (Width)	8.8”
3	Inter-Cell Flux Trap Gap	7.68”
4	Storage Cell Length	196”
5	Storage Cell Wall Thickness	0.209”
6	Neutron Absorber Material	N/A
7	Neutron Absorber Length	N/A
8	Neutron Absorber Width	N/A
9	Neutron Absorber Thickness	N/A
10	Distance from Top of Rack Baseplate to Bottom of Neutron Absorber	N/A
11	Neutron Absorber Sheathing Thickness	N/A
12	Baseplate Thickness	1”
13	Baseplate Flow Hole Diameter	5”
14	Rack Pedestal Type (Fixed or Adjustable)	Adjustable
15	Rack Pedestal Height (Female + Male)	( )
16	Rack Female Pedestal Dimensions	
	Corner Pedestals	18” x 18” x 3.5”
	Center Pedestals	10” x 10” x 3.5”
17	Rack Male Pedestal Diameter	4.5”
18	Top Plate Thickness	1”

* All of the dimensions are nominal values.

Table 2-3 Damaged Fuel Rack Data*

1	Storage Cell Center-to-Center Pitch	24”
2	Storage Cell Inner Dimension (Width)	9.25”
3	Inter-Cell Flux Trap Gap	N/A
4	Storage Cell Length	206”
5	Storage Cell Wall Thickness	0.375”
6	Neutron Absorber Material	N/A
7	Neutron Absorber Length	N/A
8	Neutron Absorber Width	N/A
9	Neutron Absorber Thickness	N/A
10	Distance from Top of Rack Baseplate to Bottom of Neutron Absorber	N/A
11	Neutron Absorber Sheathing Thickness	N/A
12	Baseplate Thickness	1”
13	Baseplate Flow Hole Diameter	N/A
14	Rack Pedestal Type (Fixed or Adjustable)	N/A
15	Rack Pedestal Height (Female + Male)	N/A
16	Rack Female Pedestal Dimensions	N/A
	Corner Pedestals	N/A
	Center Pedestals	N/A
17	Rack Male Pedestal Diameter	N/A

* All of the dimensions are nominal values.

Table 3-1 Loads and Load Combinations for Fuel Racks

Loading Combination	Service Level
$D + L$ $D + L + T_o$ $D + L + T_o + E$	Level A
$D + L + T_a + E$ $D + L + T_o + P_f$	Level B
$D + L + T_o + F_d$ $D + L + T_a + E'$	Level D†

† The functional capability of the fuel racks must be demonstrated.

Where

D = Dead weight induced loads (including fuel assembly weight)

L = Live load (not applicable for the fuel rack, since there are no moving objects in the rack load path). Note that it is accepted practice to consider the fuel weight as a dead weight.

E = Operating Basis Earthquake (OBE)

E' = Safety Shutdown Earthquake (SSE)

T_o = Differential temperature induced loads, based on the most critical transient or steady state condition under normal operation or shutdown conditions.

T_a = Differential temperature induced loads, based on the postulated abnormal design conditions.

F_d = Force caused by the accidental drop of the heaviest load from maximum possible height.

P_f = Force on the racks caused by postulated stuck fuel assembly. This force may be caused at any angle between horizontal and vertical.

Table 3-2 Material Data (ASME – Section II, Part D)

Material	Young's Modulus E (psi)	Yield Strength Sy (psi)	Ultimate Strength Su (psi)
Rack Material Data (200°F)			
SA240, Type 304L	27.6×10^6	21,400	66,100
Support Material Data (200°F)			
SA-240, Type 304L (Upper Part of Support Feet)	27.6×10^6	21,400	66,100
SA-564, Type 630 (Hardened at 1100°F)	27.8×10^6	106,300	140,000

Table 3-3 Computer Codes for US-APWR Fuel Racks Analysis

Code	Version	Description
DYNAMO Suite	1.0	All WPMR code is now grouped under one program called DYNAMO Suite. All other pre-processor and post-processor codes, which are described previous technical report (MUAP-07033P R0) are not required to be individually listed in this table.
ANSYS	14.0	Is a general purpose commercial FEA code.
LS-DYNA	971	General purpose commercial FEM code optimized for shock and impact analyses

Table 3-4 Simulation List

Run No.	Time History No	Rack	Coefficient of Friction	Seismic Input
1	Set 1	**SFR**	Random(Note 1)	SSE
2	Set 2			SSE
3	Set 3			SSE
4	Set 4			SSE
5	Set 5			SSE
1	Set 1	**NFR**	Random(Note 1)	SSE
2	Set 2			SSE
3	Set 3			SSE
4	Set 4			SSE
5	Set 5			SSE

Note 1:"Random" means that the coefficient of friction values are randomly assigned to each support pedestal based on a Gaussian distribution having a mean value of 0.5 and upper and lower bound limits of 0.8 and 0.2, respectively. See Tables 3-11 and 3-12.

Table 3-5 Summary of Time History Simulation Results

Run No.	Time History No.	Max. Stress Factor	Max. Vertical Load on Single Pedestal (lbf)	Max. Shear Load on Single Pedestal (lbf) (X or Y)	Max. Fuel to Cell Wall Impact (lbf)
SFR					
1	Set 1	0.271	579,000	259,000	1,841
2	Set 2	0.219	485,000	249,000	2,058
3	Set 3	0.247	548,000	250,000	1,473
4	Set 4	0.262	560,000	232,000	2,045
5	Set 5	0.294	519,000	251,000	1,716
Sensitivity Run					
1	Set 1	0.188	412,000	192,000	1,648
DFR					
1	Set 1	-	-	-	6,438
NFR					
1	Set 1	0.121	195,000	95,000	5,254
2	Set 2	0.119	195,000	102,000	5,413
3	Set 3	0.105	164,000	112,000	5,477
4	Set 4	0.135	220,000	101,000	5,159
5	Set 5	0.183	299,000	142,000	5,350

Table 3-6 Rack Displacements

Time History No.	Location on Rack	Maximum Rack Displacement Relative to floor (inch)	COF
SFR			
Set 1	Base Plate	0.68	Random
Set 1	Top of Rack	3.93	
Sensitivity Run			
Set 1	Base Plate	0.30	Random
Set 1	Top of Rack	2.29	
NFR			
Set 5	Base Plate	0.71	Random
Set 3	Top of Rack	0.59	

Table 3-7 Rack Impact Loads

	Maximum Impact Load on One Side of Rack (lbf)	Location of Rack
SFR		
Rack-to-Rack	No Impact / 396,600	Base Plate / Top Corner
Rack-to-Wall	No Impact	-
NFR		
Rack-to-rack	151,500 / 465,000	Base Plate / Top Corner
Rack-to-Wall	658,100	Adjustable Support

Table 3-8 Maximum Stress Factors

	Pedestal Stress Factor	Cell Wall Stress Factor
SFR	0.194	$\left(0.294\times(\frac{1}{0.758})\right)=0.388$ *1
NFR	0.061	0.183*2

Note 1: Adjustment factor accounting for ASME Code slenderness ration evaluation.
Note 2: Since the with-thickness ratio of NFR is not greater than 51.4, no additional adjustment for the stress is necessary. Therefore the stress factor of 0.183 is considered as the maximum stress factor.

Table 3-9 Stress Evaluation for Fuel Racks

Region	Type	Stress (psi)	Allowable Stress (psi)	Safety Factor (-)
SFR				
Baseplate-to Rack Cell	Weld	21,430	35,694	1.66
Baseplate-to-Pedestal	Weld	18,118	35,694	1.97
	Base Metal Shear	12,811	15408	1.20
Cell-to-Cell	Weld	5,908	35,694	6.04
	Base Metal Shear	4,178	15,408	3.68
Pedestal Thread	Shear	12,037	15,408	1.28
Top Plate	Compression	5,691	21,400	-
	Weld	17,113	35,694	2.08
Bearing Pad	Vertical Compression	5,790	21,400	-
	Horizontal Compression	6,267	21,400	-
NFR				
Baseplate-to Rack Cell	Weld	15,199	35,694	2.34
Baseplate-to-Pedestal	Weld	18,208	35,694	1.96
	Base Metal Shear	12,875	15,408	1.19
Cell-to-Cell	Weld	14,683	35,694	2.43
	Base Metal Shear	10,382	15,408	1.48
Pedestal Thread	Shear	9,732	15,408	1.58
Adjustable Support Thread	Shear	12,014	15,408	1.28
Adjustable Support-to Top Plate	Weld	30,266	35,694	1.17
Top Plate	Compression	3,875	21,400	-
	Weld	3,963	35,694	9.00
Baseplate	Compression	2,690	21,400	-

Table 3-10 Level A Maximum Pedestal Load

Item	Load (lbf)
Dry Weight of 13x12 Rack	63,818
Dry Weight of 156 Intact Fuel Assemblies	298,272
Total Dry Weight	362,090
Load per Pedestal	90,523

Table 3-11 Coefficients of Friction for Spent Fuel Rack

Rack No.	Pedestal No.	Coefficient of Friction	
		x	y
Rack 1	Pedestal 1	0.5116251	0.4661419
	Pedestal 2	0.3889132	0.4110418
	Pedestal 3	0.3906849	0.6666080
	Pedestal 4	0.4886670	0.6982352
Rack 2	Pedestal 1	0.4415396	0.5781227
	Pedestal 2	0.7894890	0.4093477
	Pedestal 3	0.4375129	0.4027123
	Pedestal 4	0.7595068	0.2035509
Rack 3	Pedestal 1	0.4545223	0.4380071
	Pedestal 2	0.5496646	0.5597262
	Pedestal 3	0.5586227	0.4747105
	Pedestal 4	0.4564697	0.5236342
Rack 4	Pedestal 1	0.5505734	0.5837699
	Pedestal 2	0.4153478	0.5940759
	Pedestal 3	0.4968461	0.5603341
	Pedestal 4	0.4985339	0.5638636
Rack 5	Pedestal 1	0.4638699	0.4765281
	Pedestal 2	0.5008494	0.5067566
	Pedestal 3	0.5181165	0.3827122
	Pedestal 4	0.4907442	0.4873038
Rack 6	Pedestal 1	0.4602348	0.3579084
	Pedestal 2	0.5346046	0.5726167
	Pedestal 3	0.6813118	0.5157147
	Pedestal 4	0.4325717	0.5604752

Table 3-12 Coefficients of Friction for New Fuel Rack

Rack No.	Pedestal No.	Coefficient of Friction	
		x	y
Rack 1	Pedestal 1	0.5832139	0.5210782
	Pedestal 2	0.5379882	0.5824727
	Pedestal 3	0.5717784	0.3214971
	Pedestal 4	0.4256627	0.4049447
	Pedestal 5	0.4835469	0.6050852
Rack 2	Pedestal 1	0.4914664	0.4503435
	Pedestal 2	0.4428460	0.4591069
	Pedestal 3	0.5620371	0.4631965
	Pedestal 4	0.5289003	0.6903631
	Pedestal 5	0.3625370	0.5404225
Rack 3	Pedestal 1	0.7276508	0.5527967
	Pedestal 2	0.4890727	0.4892025
	Pedestal 3	0.5303365	0.5481229
	Pedestal 4	0.6161805	0.3322129
	Pedestal 5	0.4225656	0.5690342
	Pedestal 6	0.3116830	0.4964729

Table 4-1 Impact Event Data

Drop Event	Rack Type	Impactor Weight (lbf)	Drop Height (in)	Impact Velocity (in/sec)
Shallow Drop Event	SFR	2,450	24” above top-of-rack	123.8
Deep Drop Scenario 1 (Away from Support Leg)	SFR	2,450	36” above top-of-rack	300.0
Deep Drop Scenario 2 (Above Support Leg)	SFR	2,450	36” above top-of-rack	120.0

Table 4-2 Material Properties of Rack Structural for Mechanical Analysis

	Material Data (200°F)	
	SA240, Type 304L	SA-564, Type 630 (Hardened at 1100°F)
Yield Stress (psi)	21,400	106,300
Ultimate Stress (psi)	66,100	140,000
Young’s Modulus (psi)	27.6×10^6	27.8×10^6
Failure Strain / Elongation (in/in)	0.38 *	0.14

Note: * The ASME Code lists a higher failure strain of 0.40; the use of a smaller value is conservative for the impact damage evaluation.

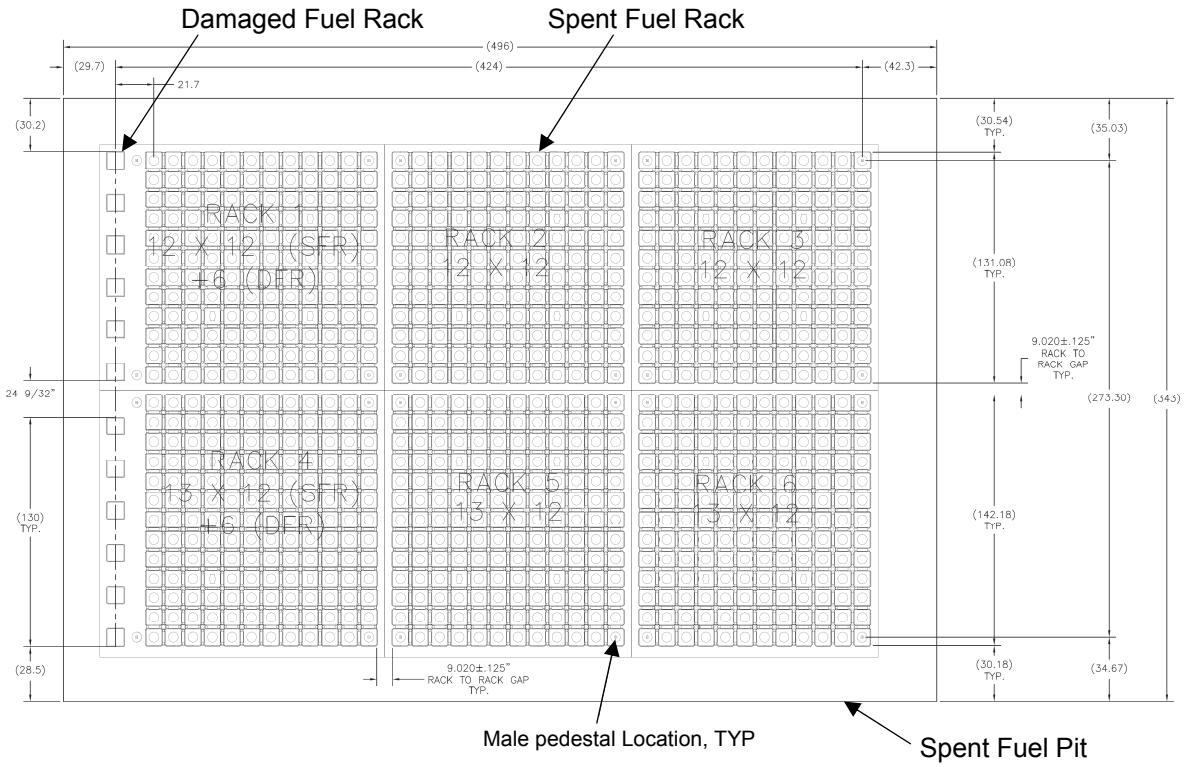

(1) Spent Fuel Rack Layout

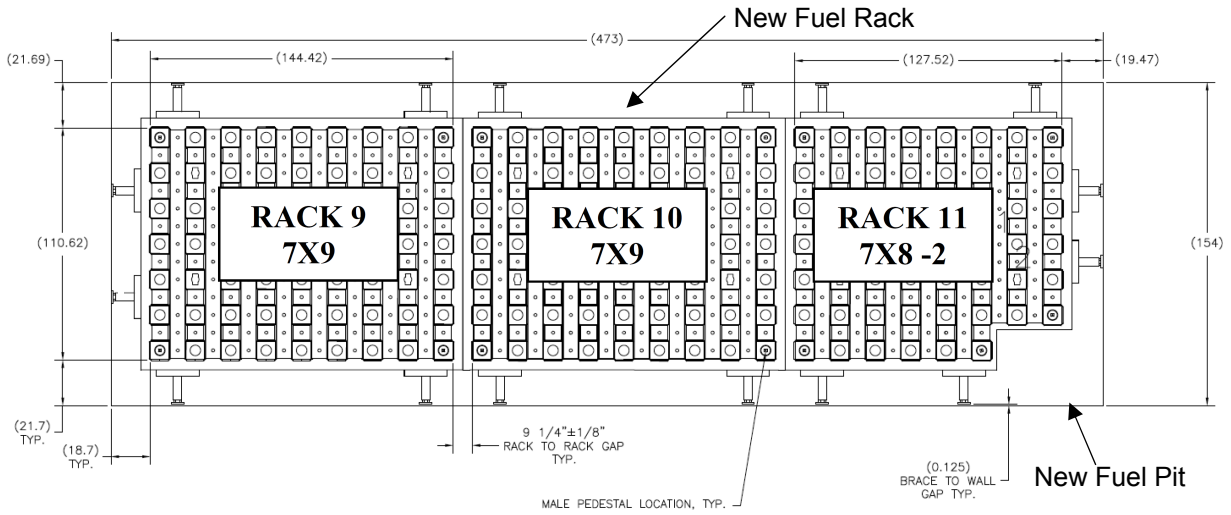

(2) New Fuel Rack Layout

Figure 2-1 Layout of US-APWR Fuel Storage

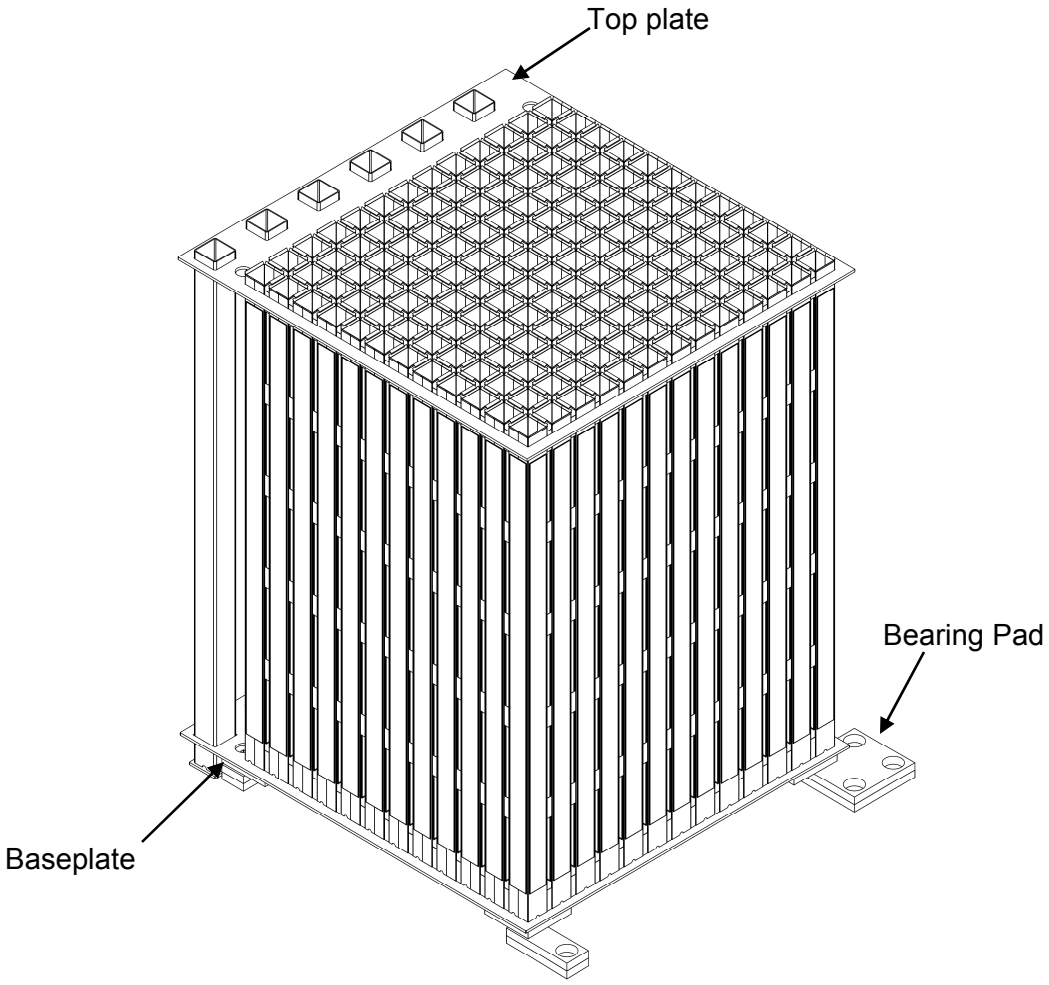

Figure 2-2 Outline of Spent Fuel Rack

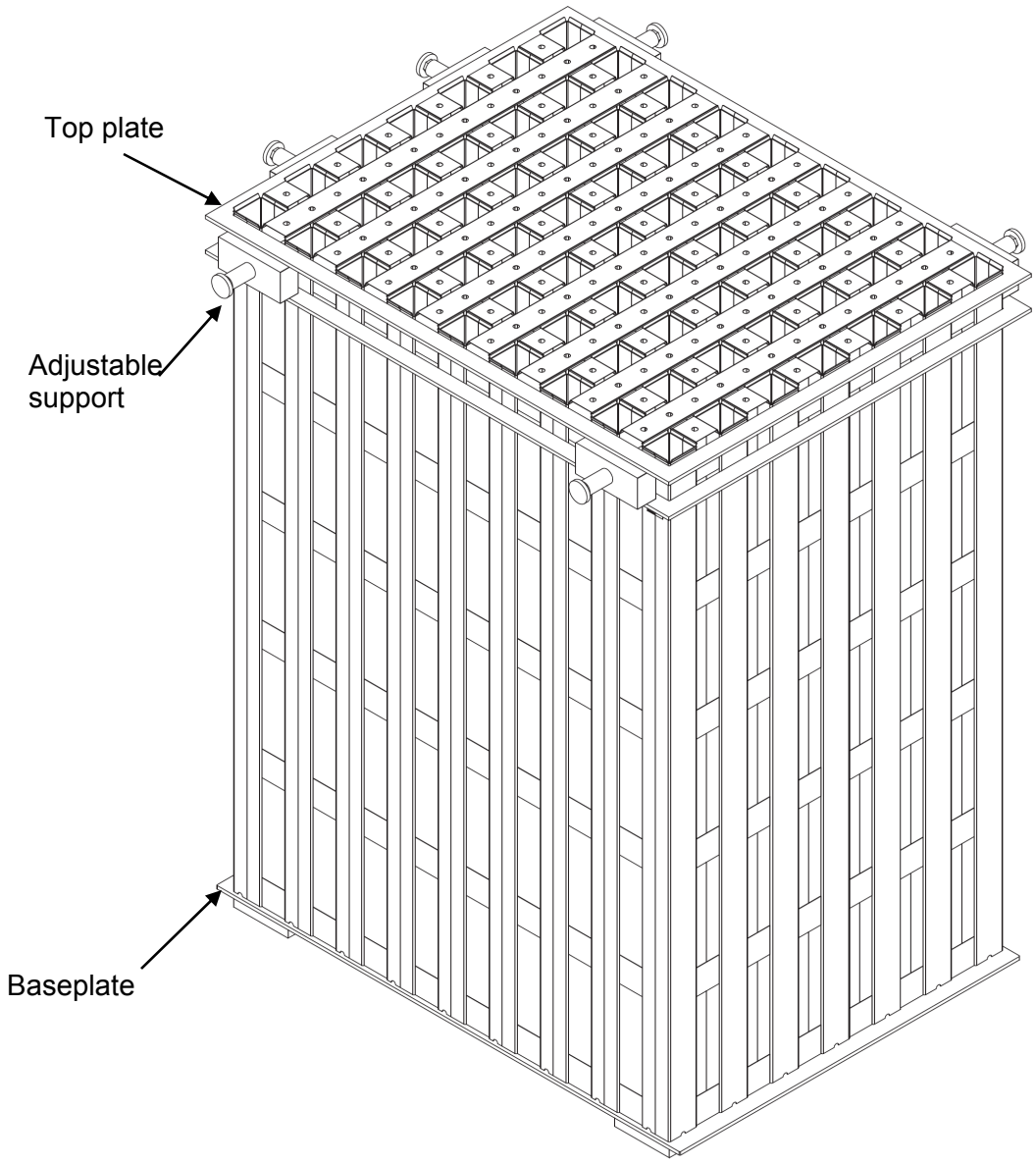

Figure 2-3 Outline of New Fuel Rack

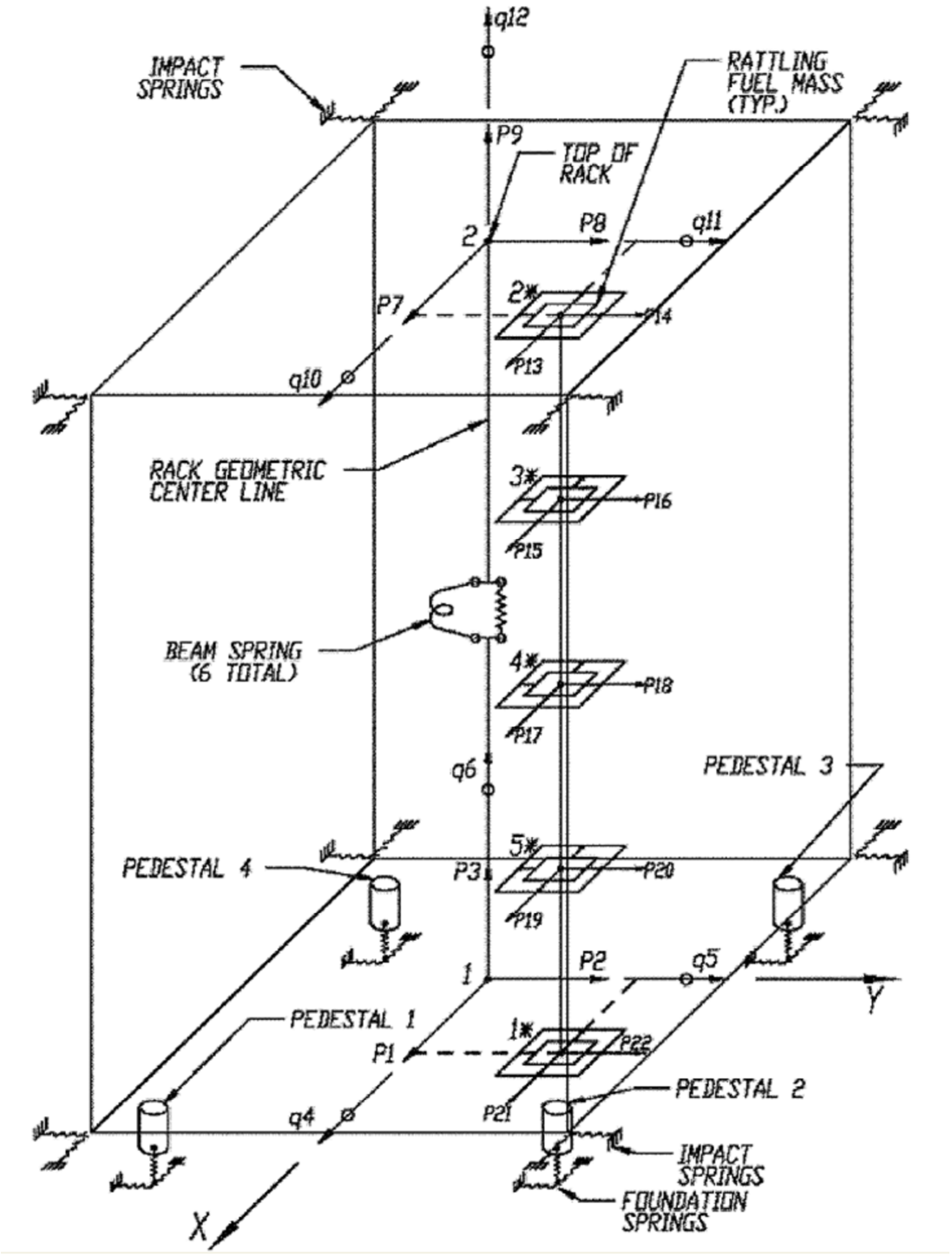

Note: The center pedestal (Pedestal 5) is not shown.

Figure 3-1 Schematic of the Dynamic Model for Dynarack

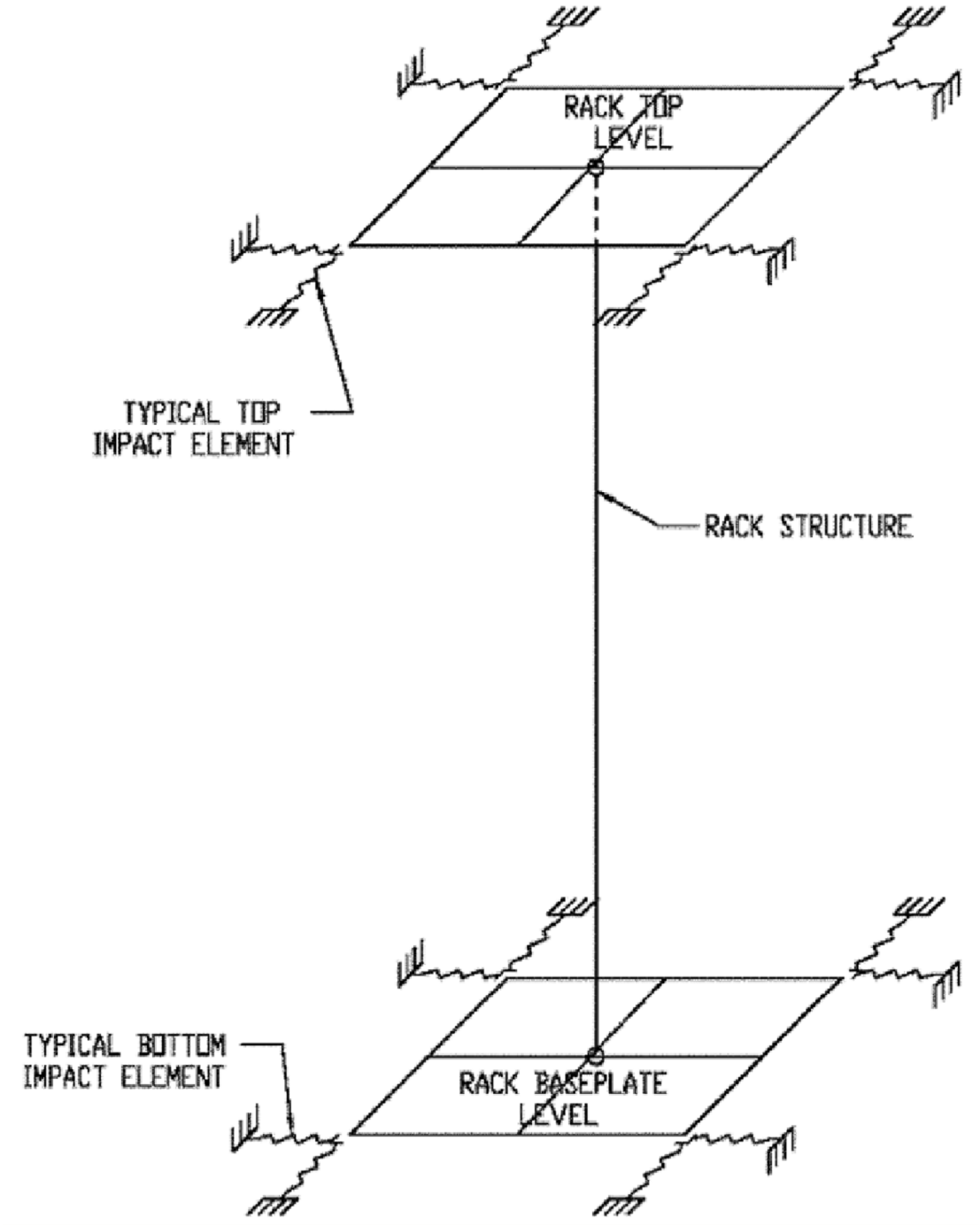

Figure 3-2 Rack-to-Rack Impact Springs

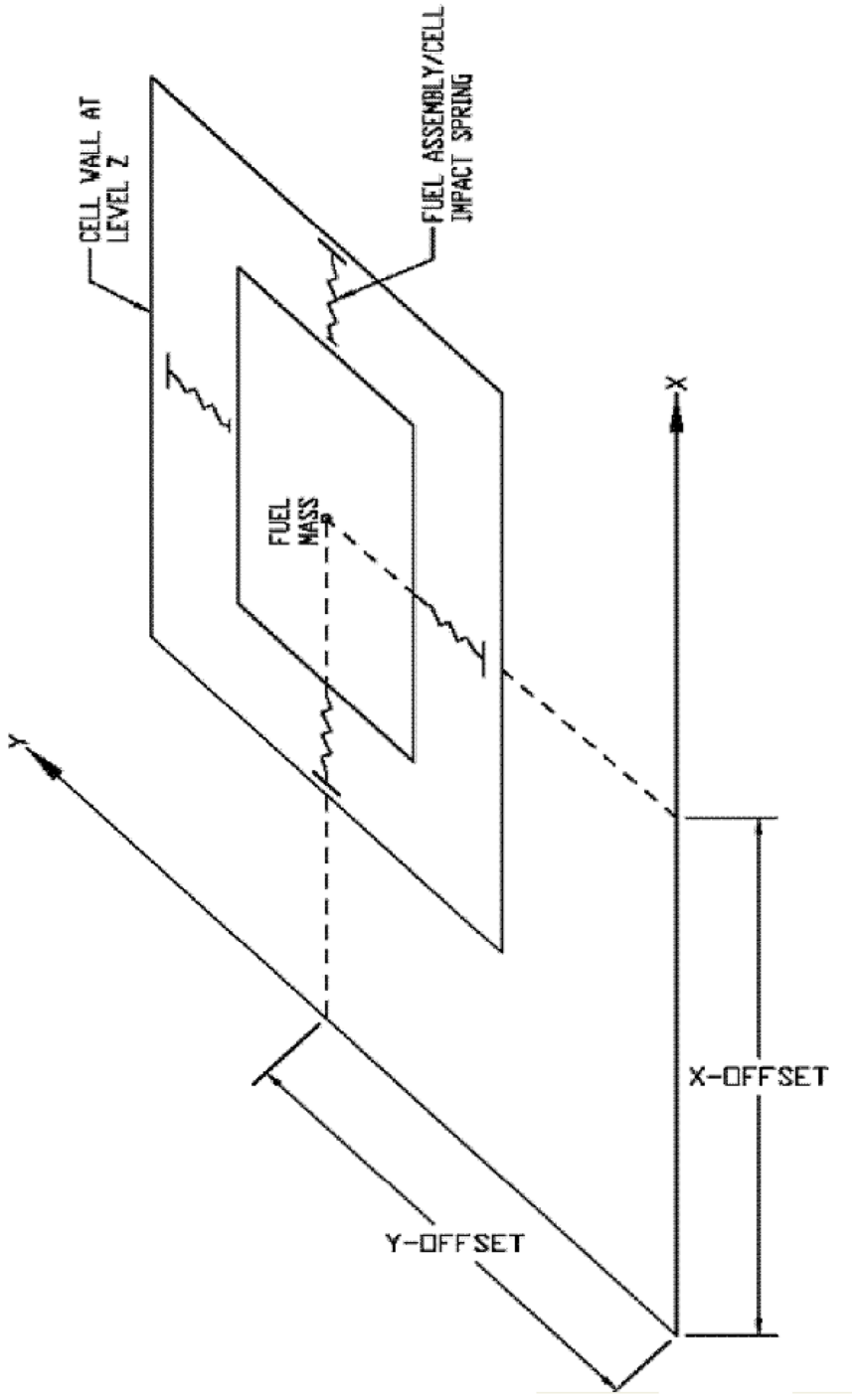

Figure 3-3 Fuel-to-Rack Impact Springs at Level of Rattling Mass

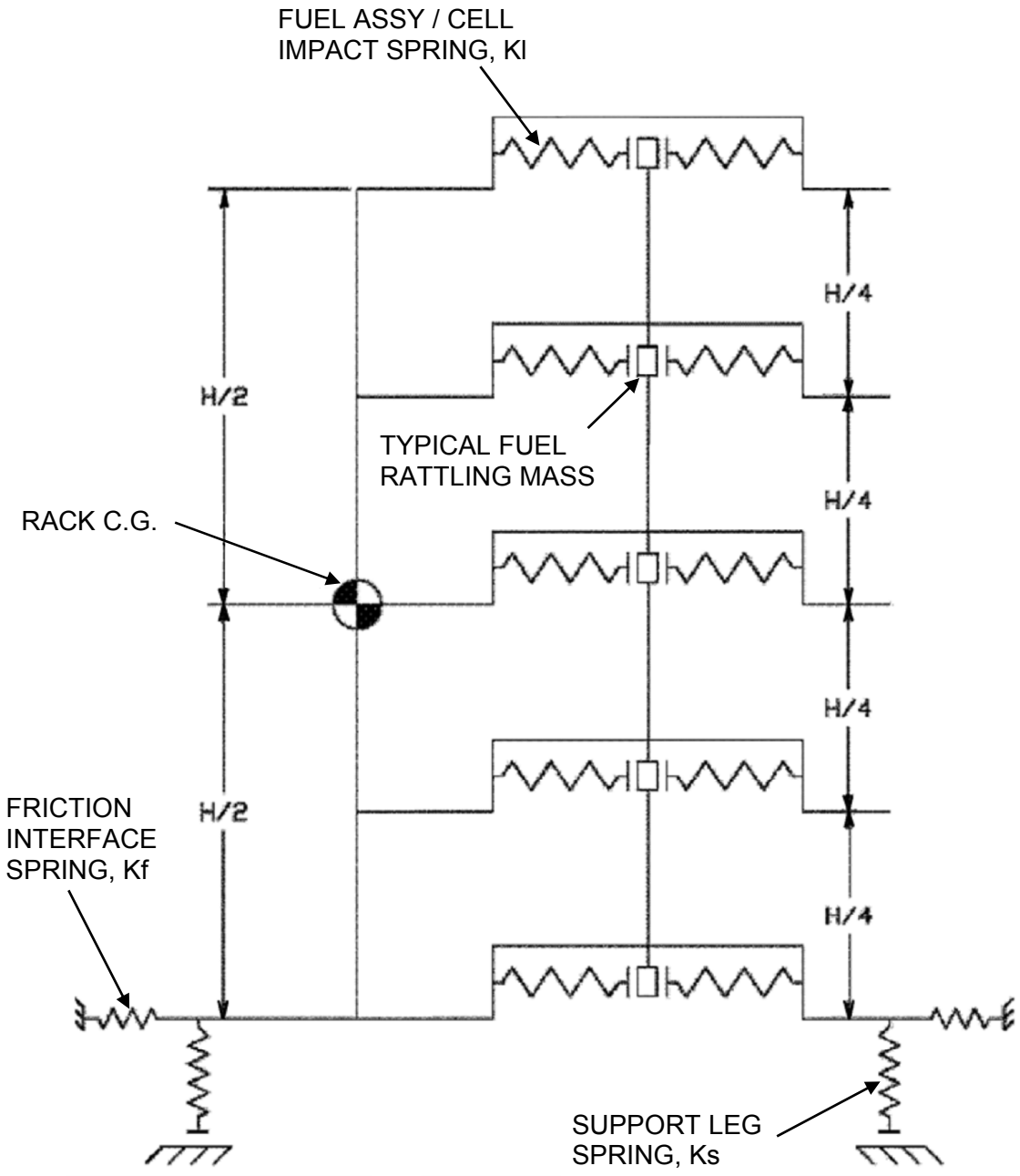

Figure 3-4 Two Dimensional View of the Spring-Mass Simulation

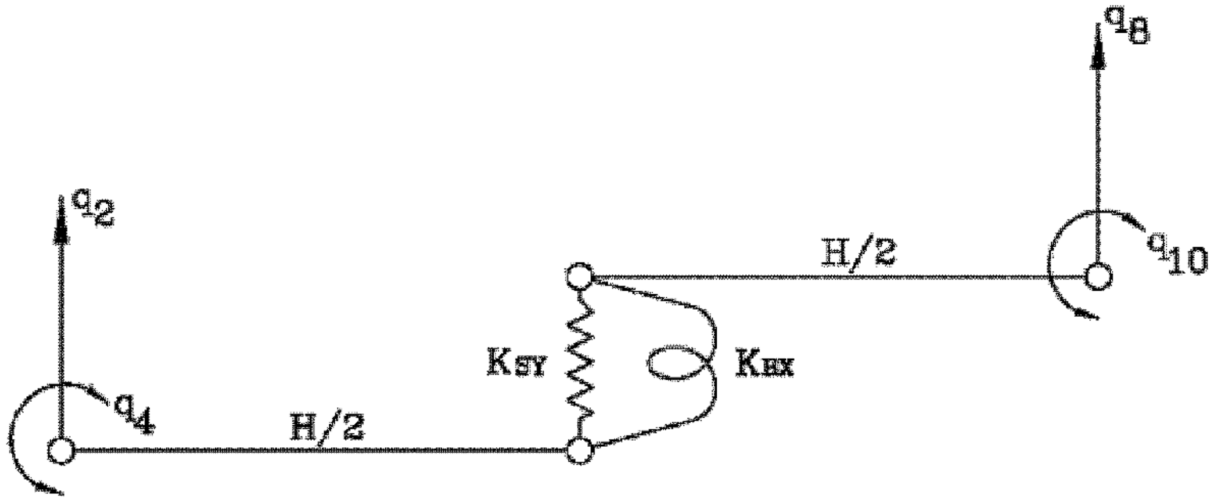

(1) Y-Z Plane Bending with Shear and Bending Spring

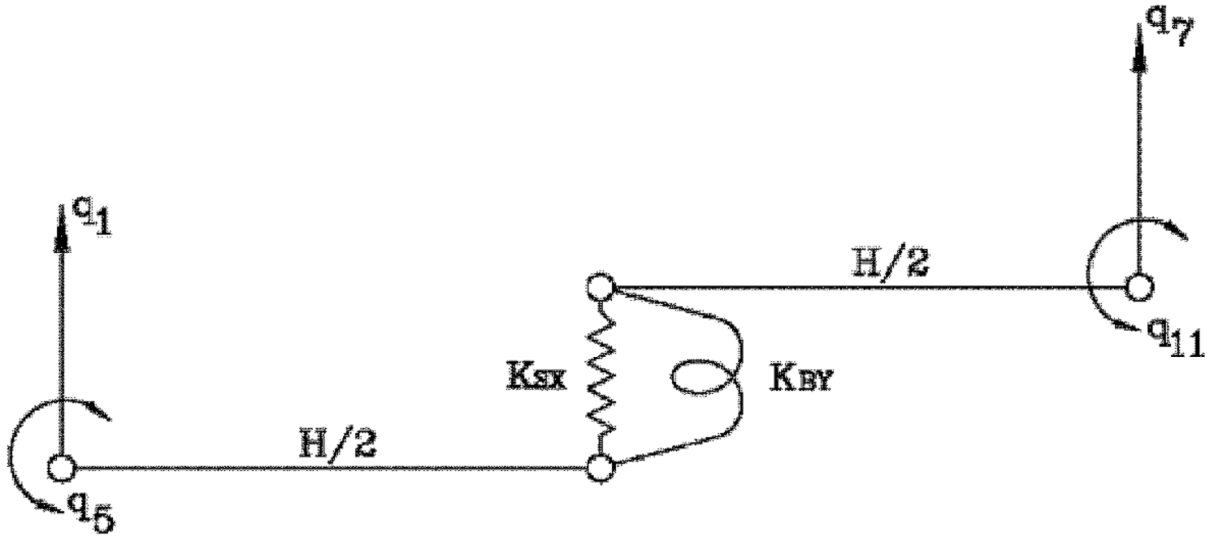

(2) X-Z Plane Bending with Shear and Bending Spring

Figure 3-5 Rack Degrees-of-Freedom

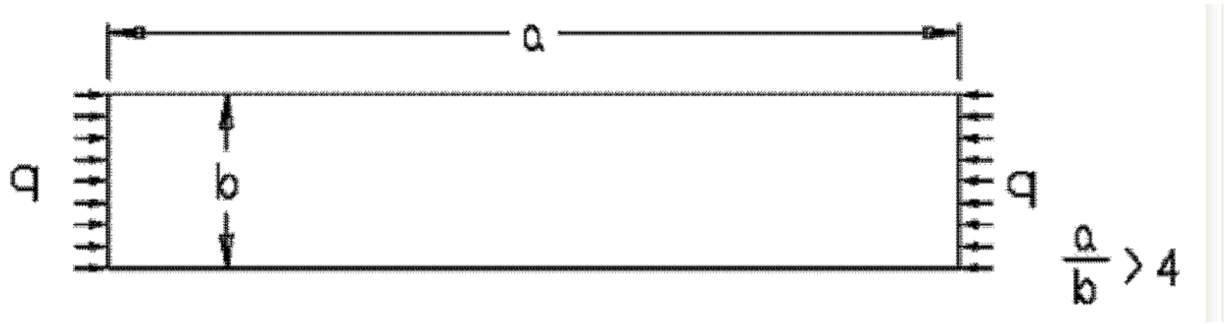

Figure 3-6 Loading on Rack Wall

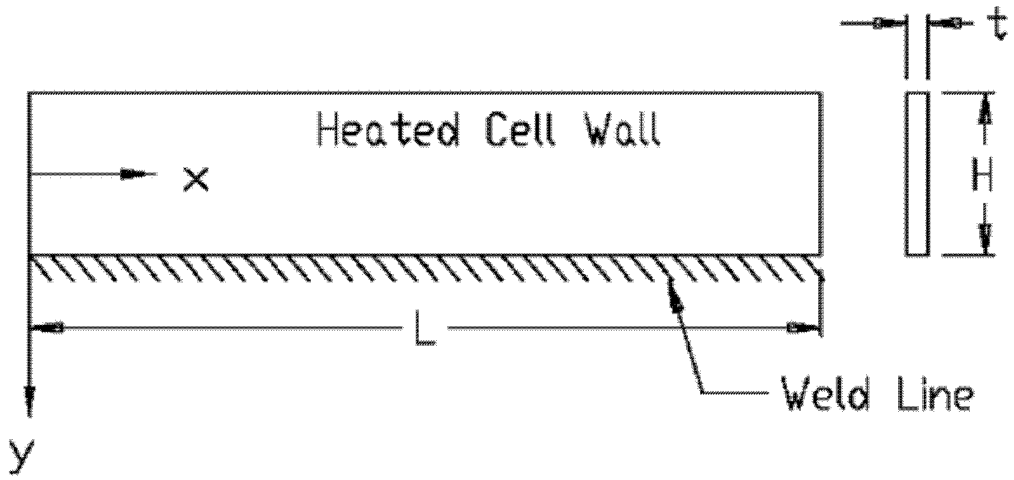

Figure 3-7 Welded Joint in Rack

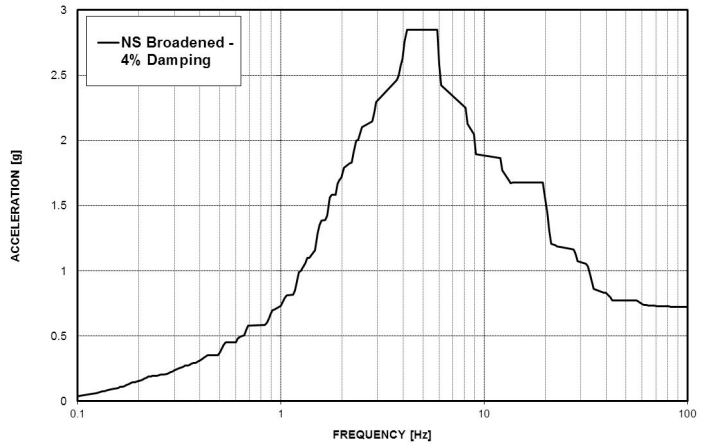

(NS-direction)

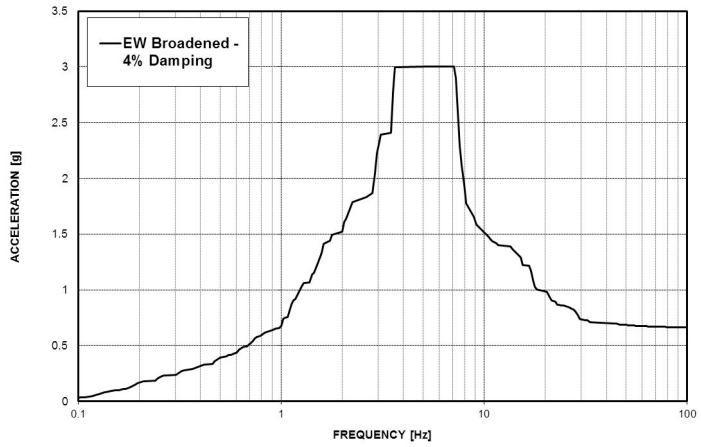

(EW-direction)

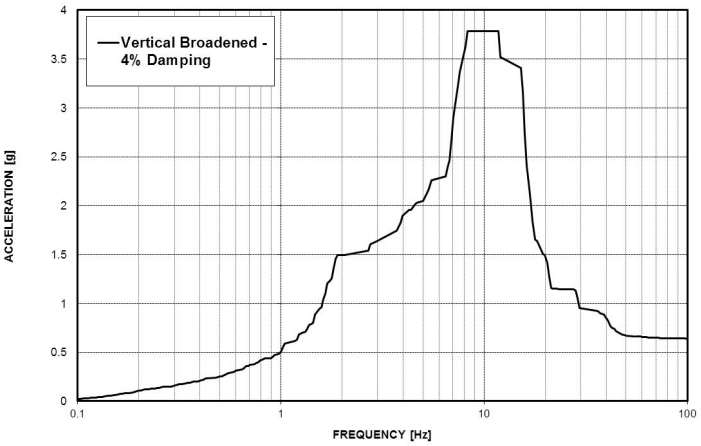

(Vertical-direction)

Figure3-8 Response Spectra for Spent Fuel Rack

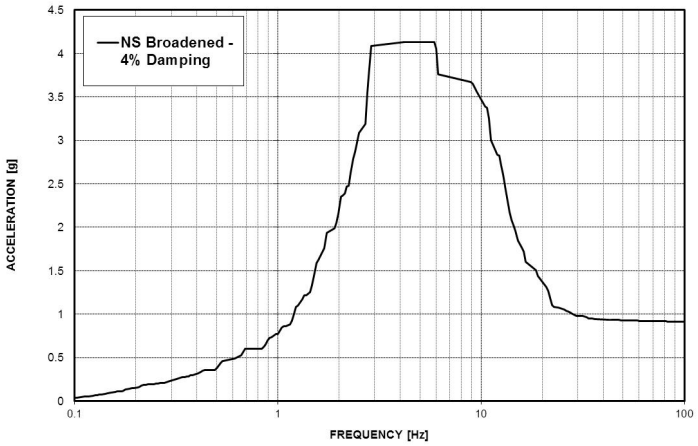

(NS-direction)

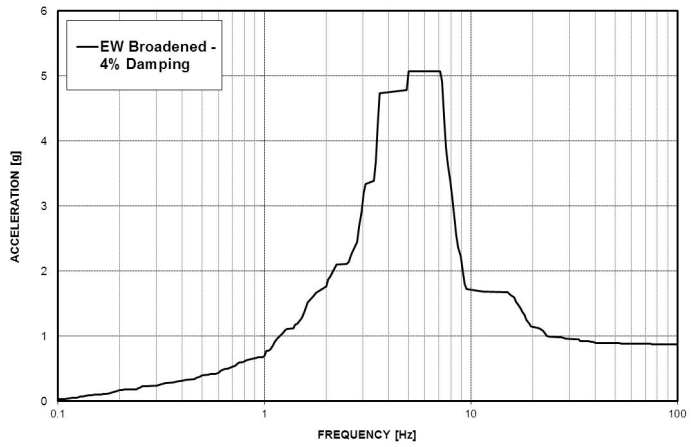

(EW-direction)

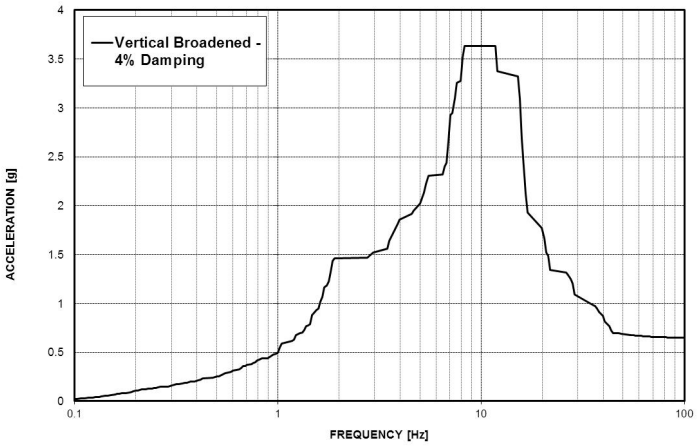

(Vertical-direction)

Figure3-9 Response Spectra for New Fuel Rack

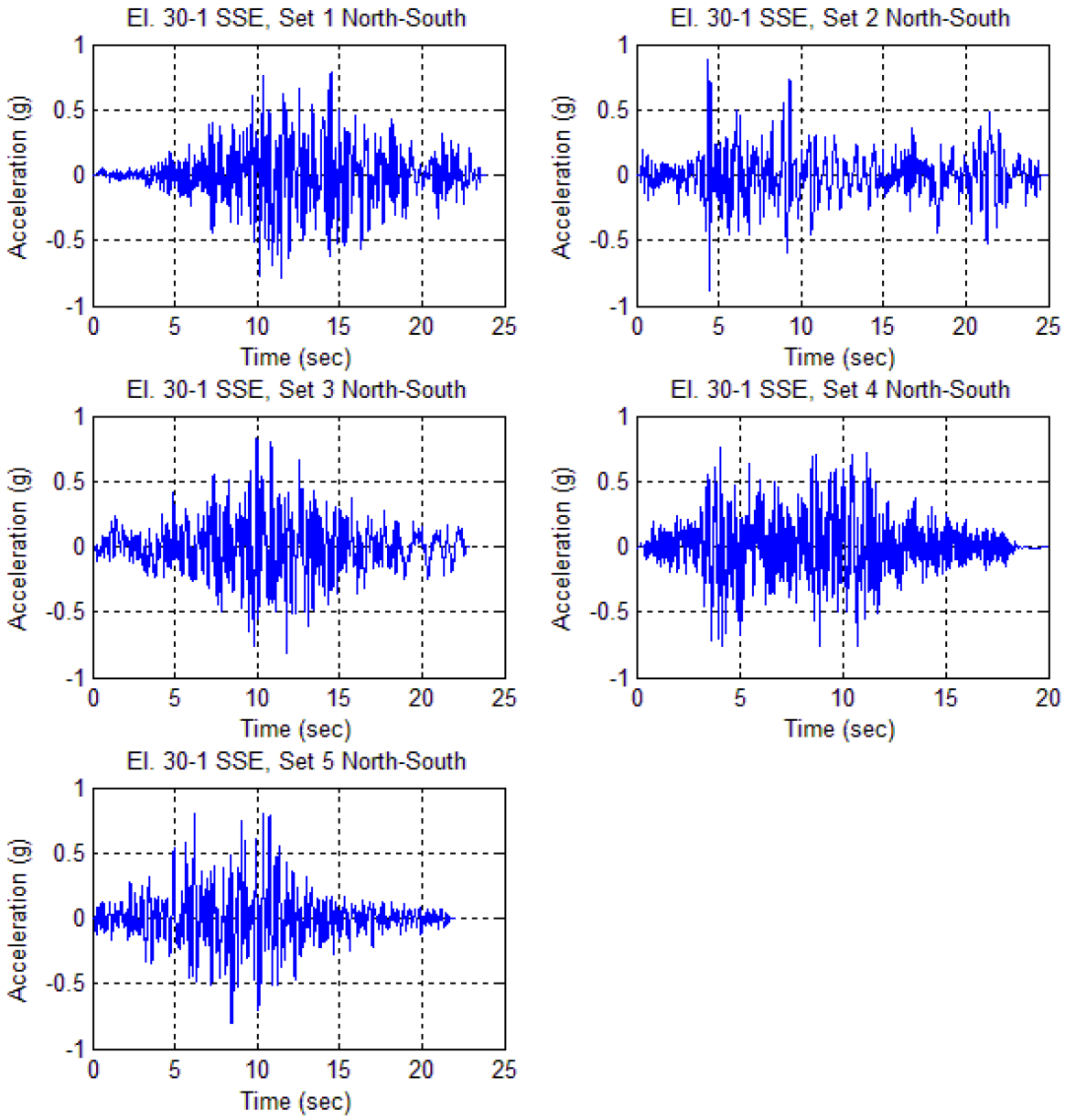

Figure 3-10 Spent Fuel Rack North-South Acceleration Time Histories

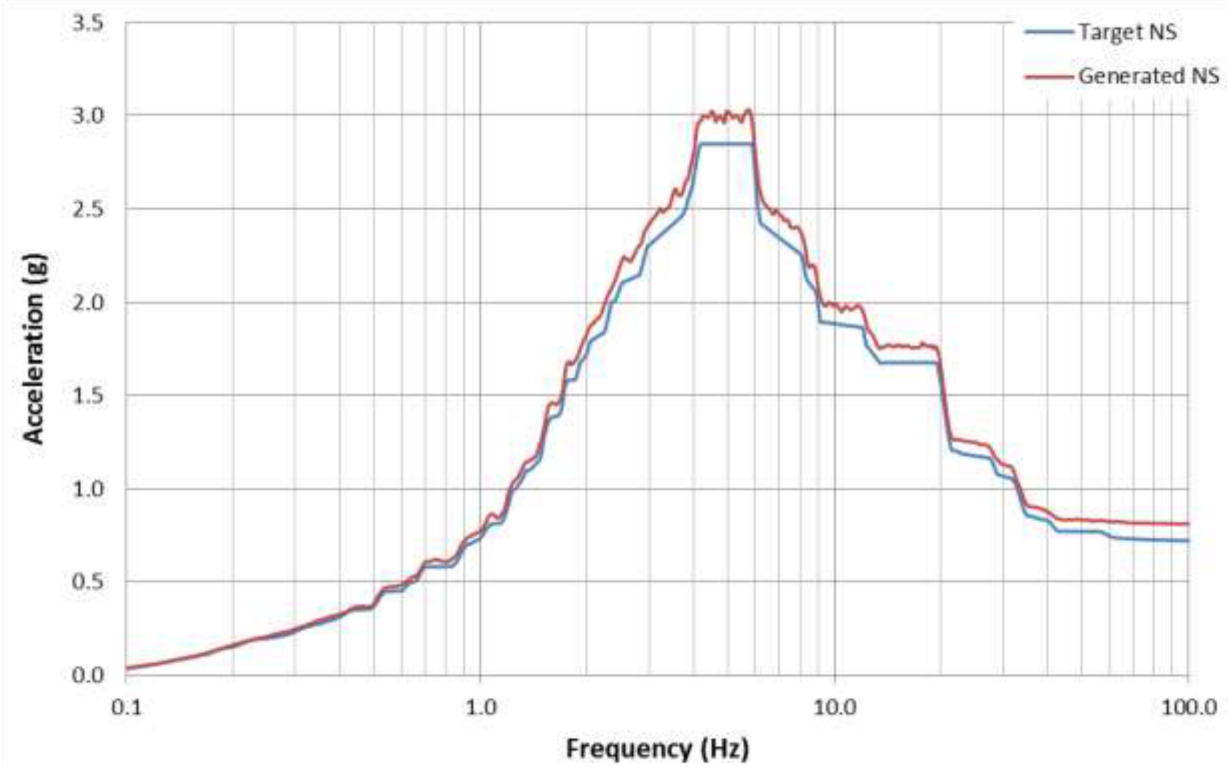

Figure 3-11 Spent Fuel Rack North-South Average Generated Response Spectra

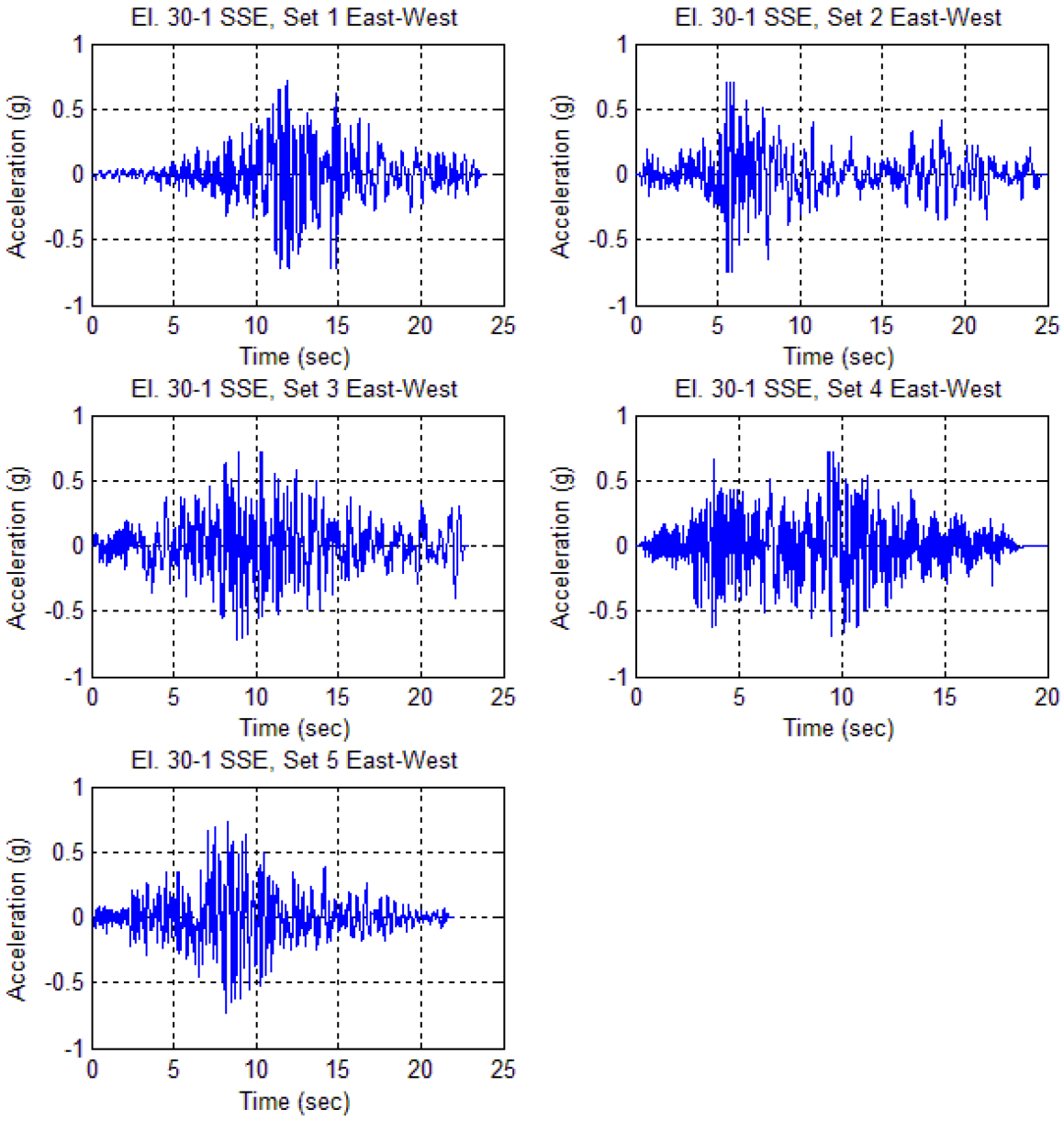

Figure 3-12 Spent Fuel Rack East-West Acceleration Time Histories

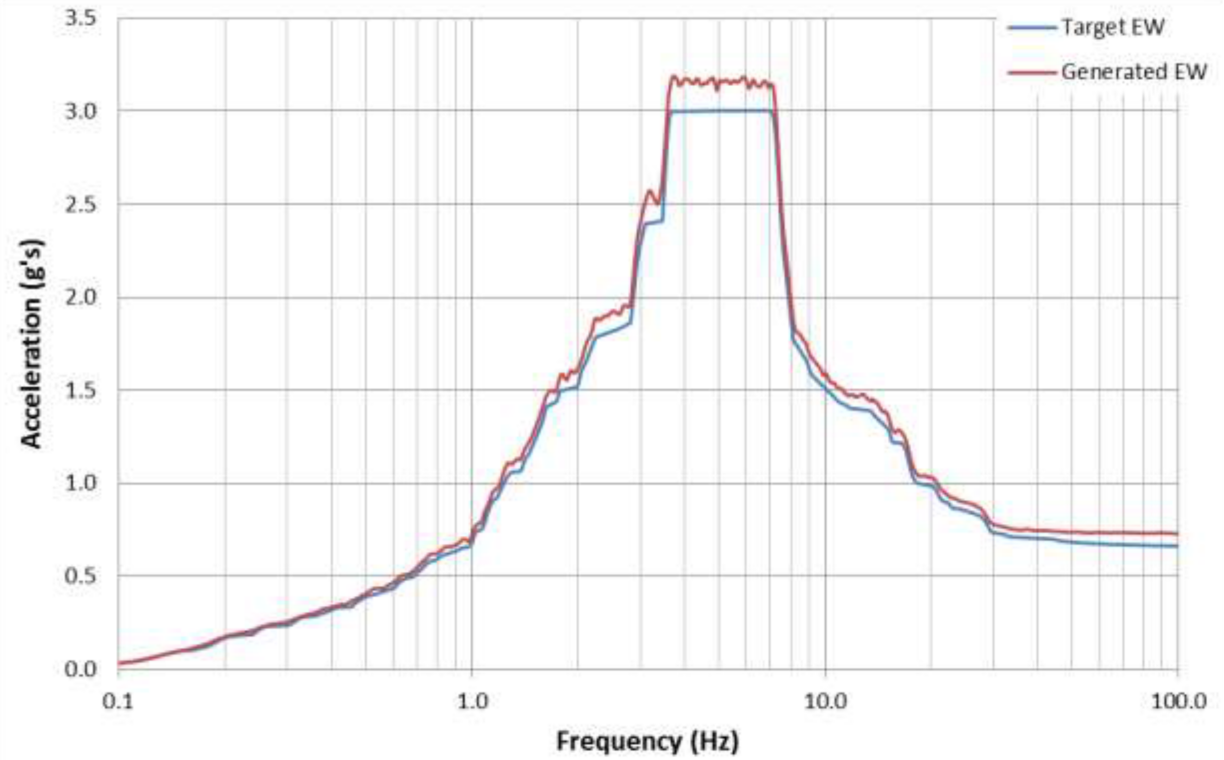

Figure 3-13 Spent Fuel Rack East-West Average Generated Response Spectra

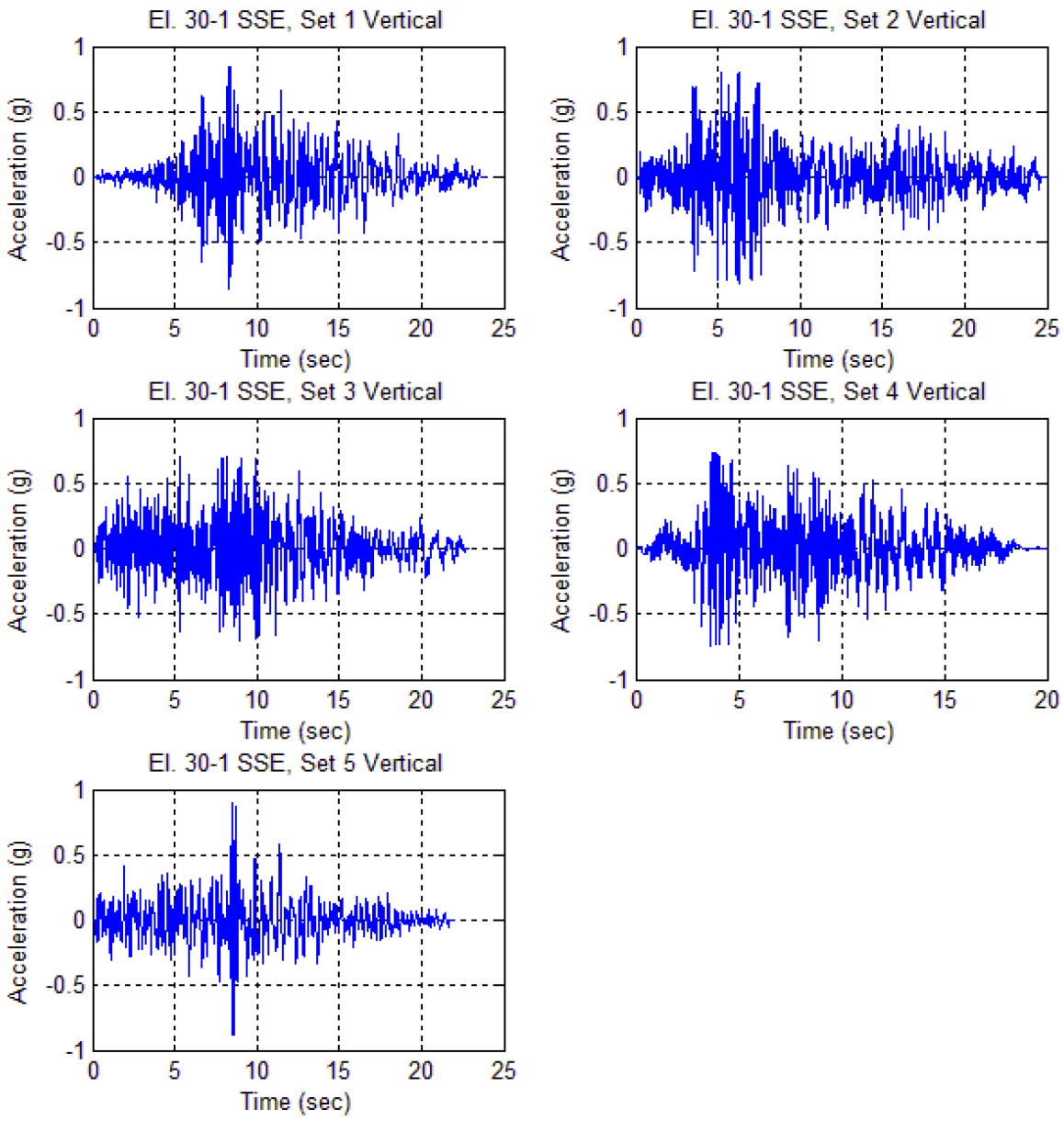

Figure 3-14 Spent Fuel Rack Vertical Acceleration Time Histories

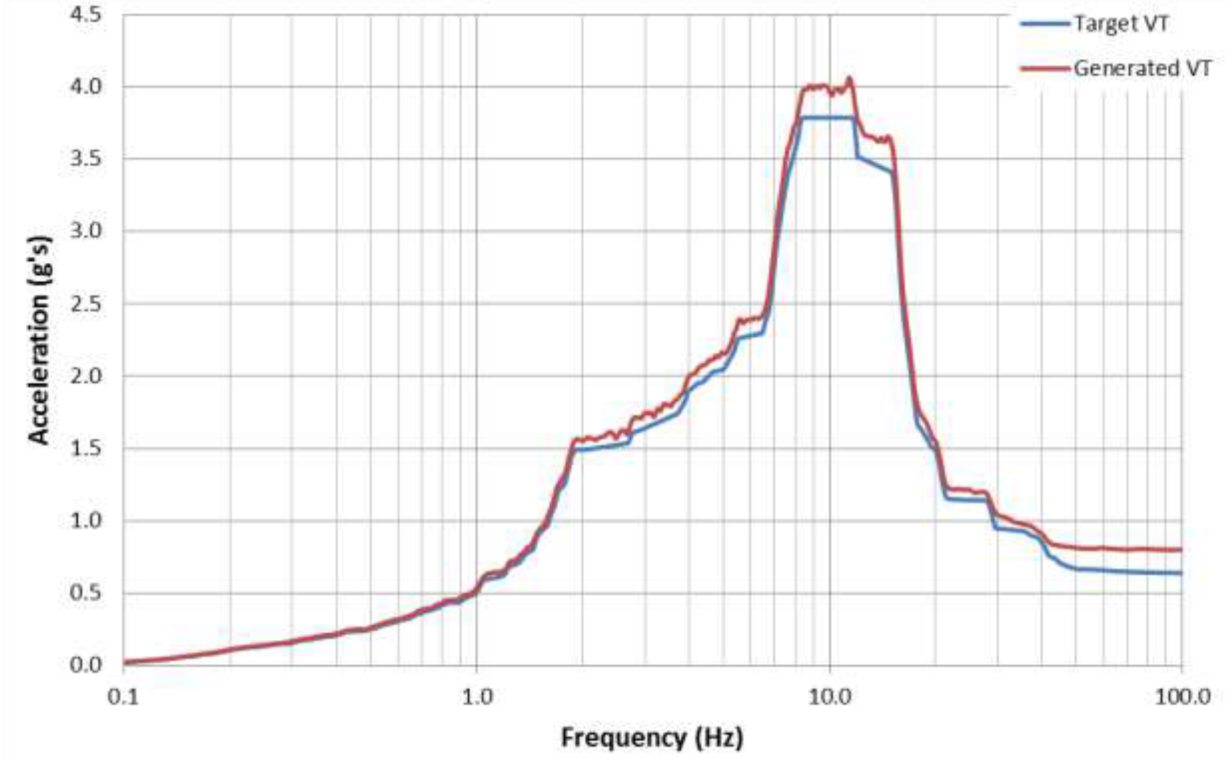

Figure 3-15 Spent Fuel Rack Vertical Average Generated Response Spectra

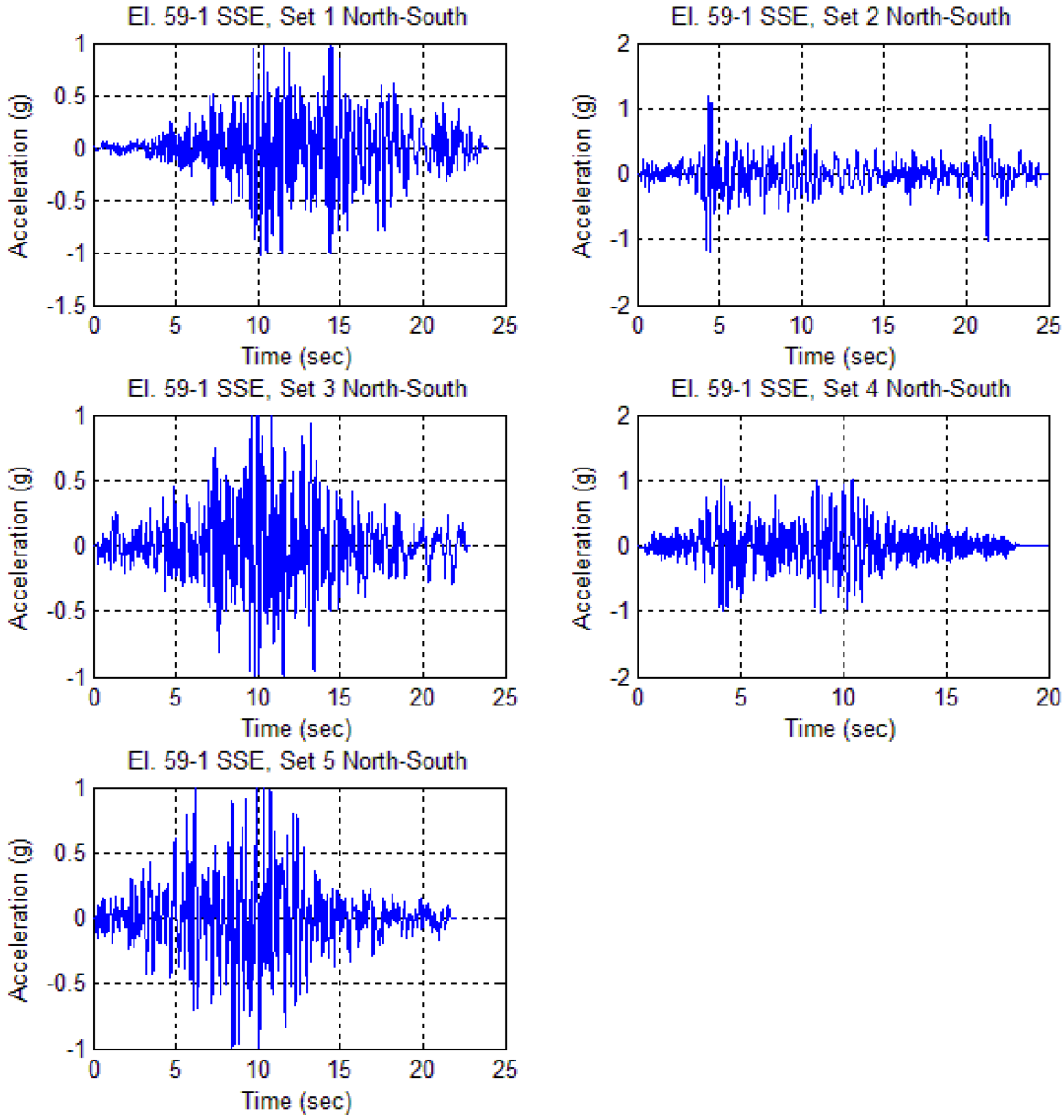

Figure 3-16 New Fuel Rack North-South Acceleration Time Histories

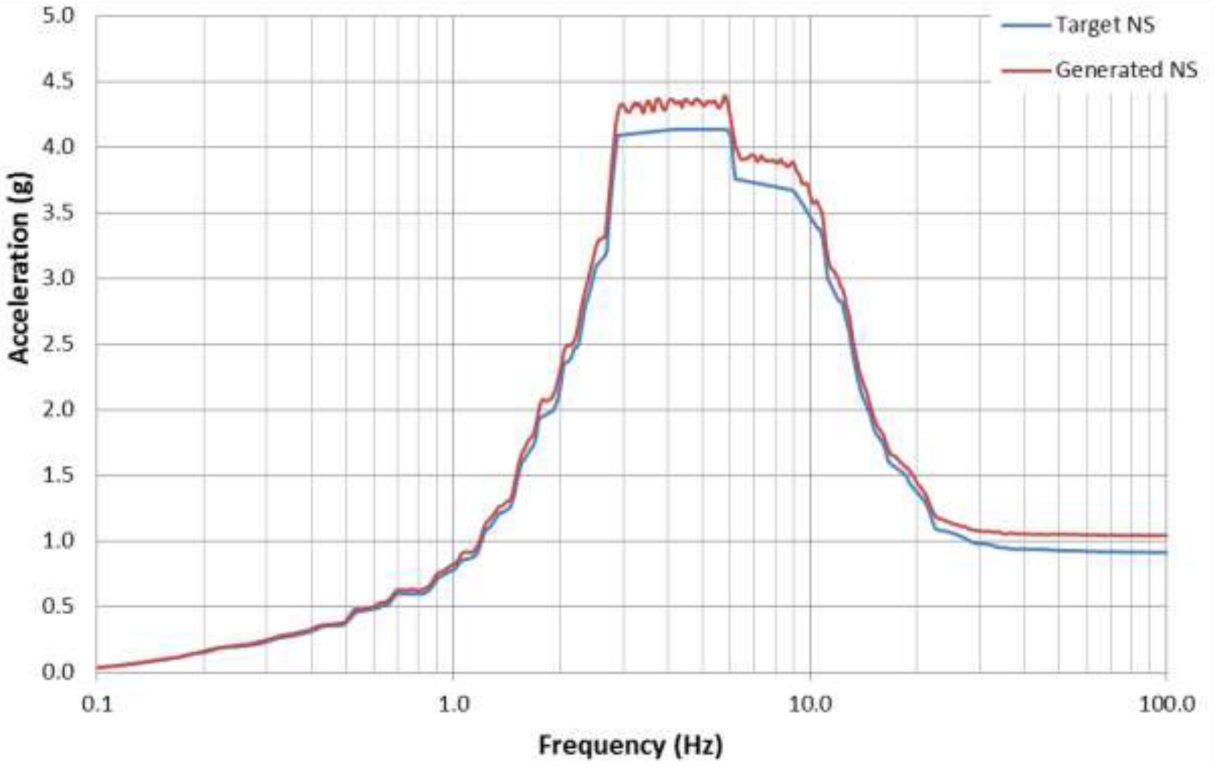

Figure 3-17 New Fuel Rack North-South Average Generated Response Spectra

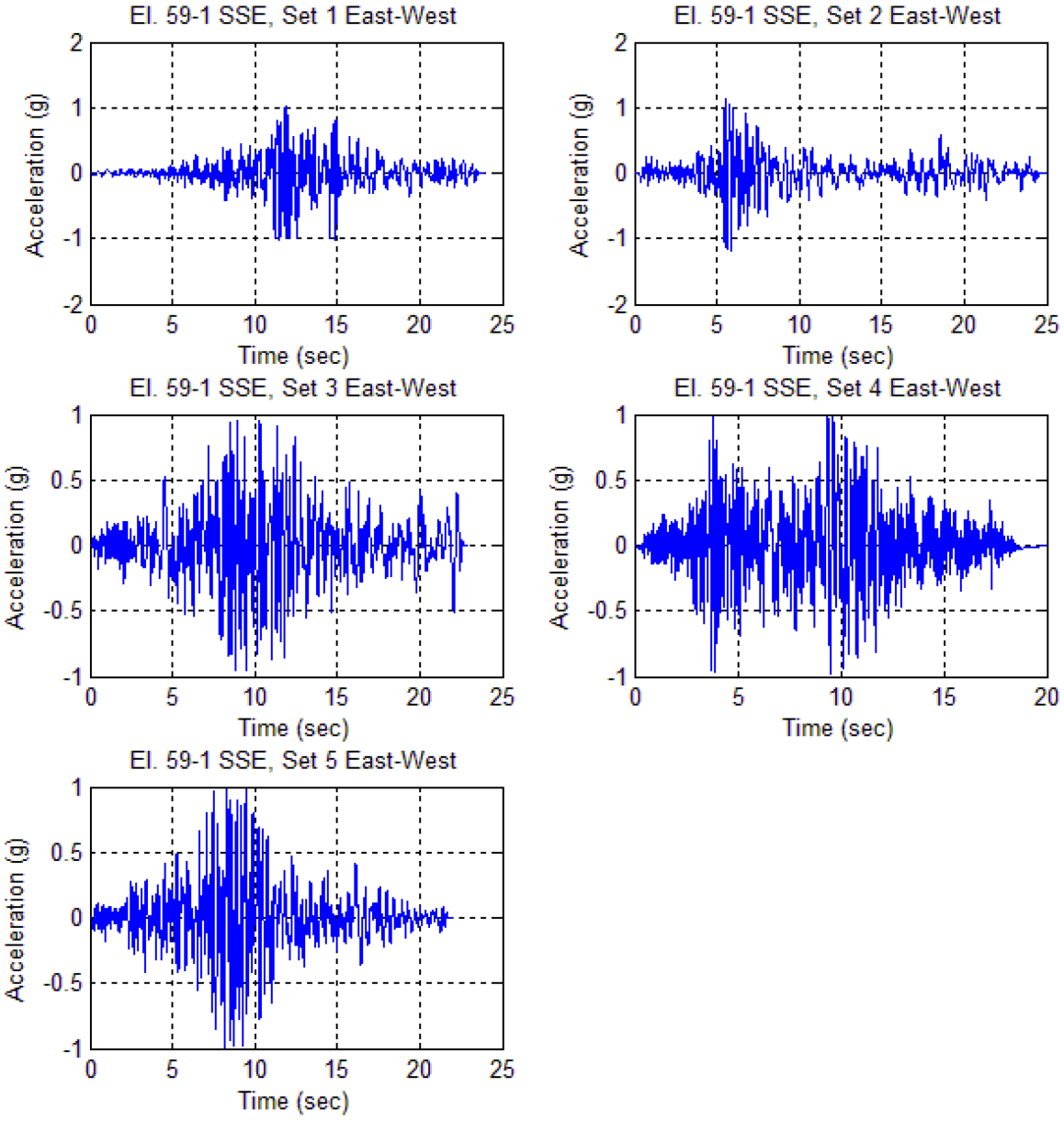

Figure 3-18 New Fuel Rack East-West Acceleration Time Histories

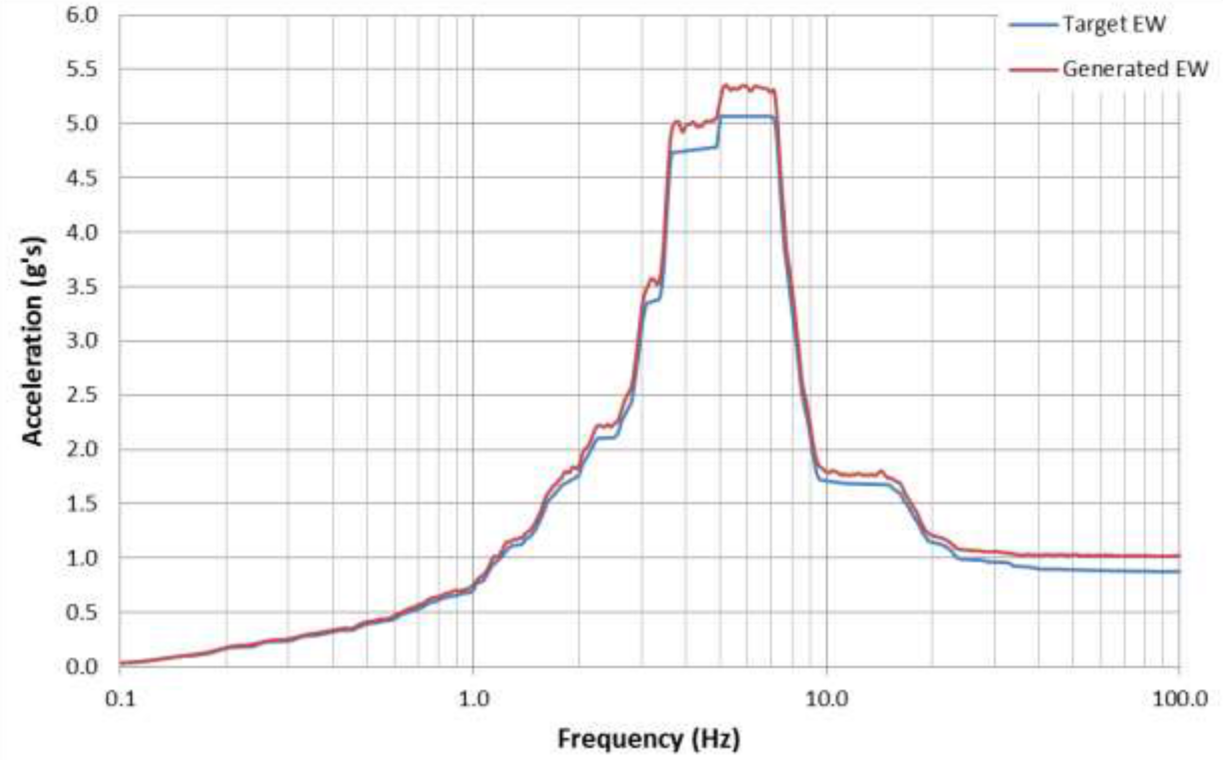

Figure 3-19 New Fuel Rack East-West Average Generated Response Spectra

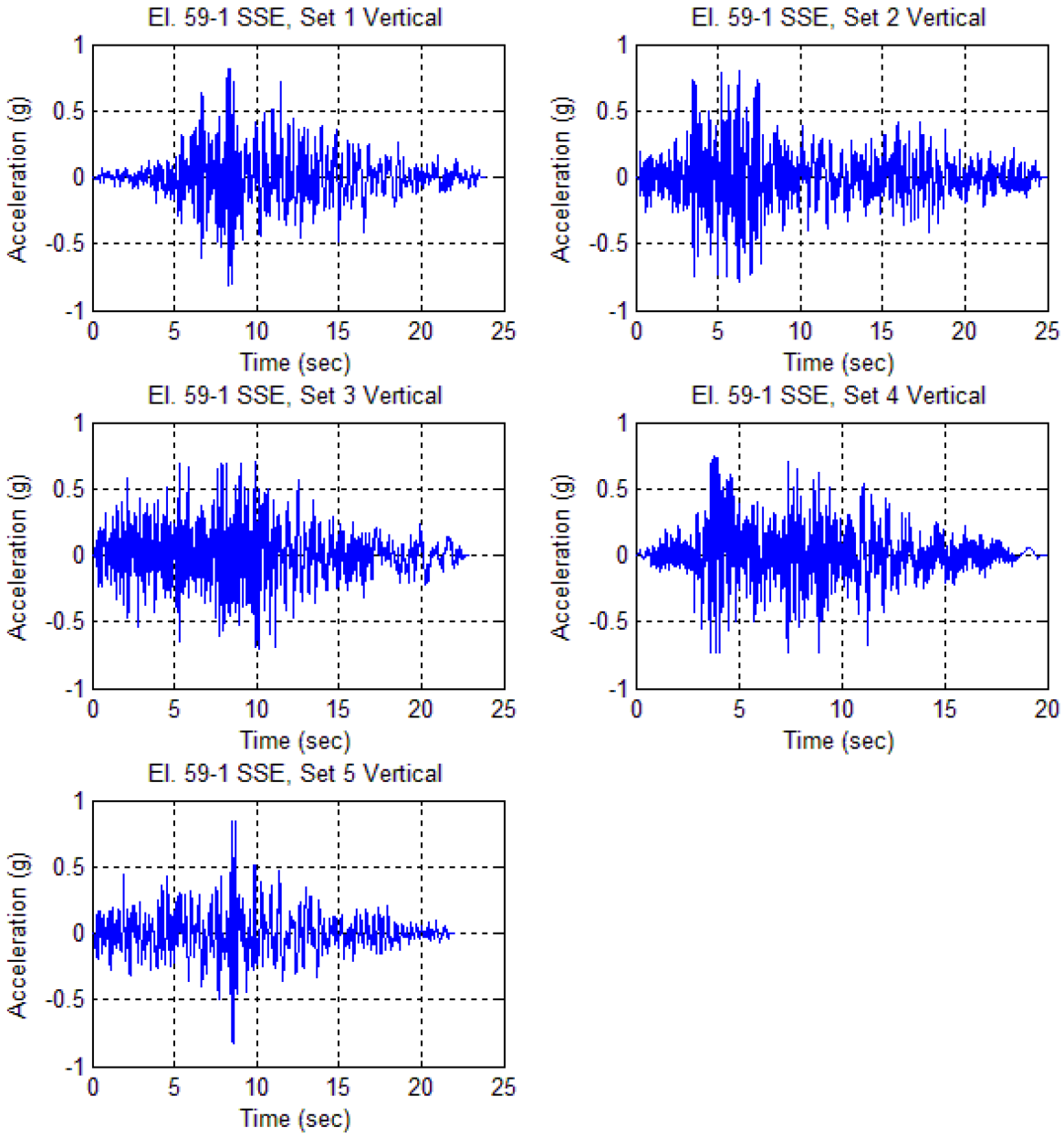

Figure 3-20 New Fuel Rack Vertical Acceleration Time Histories

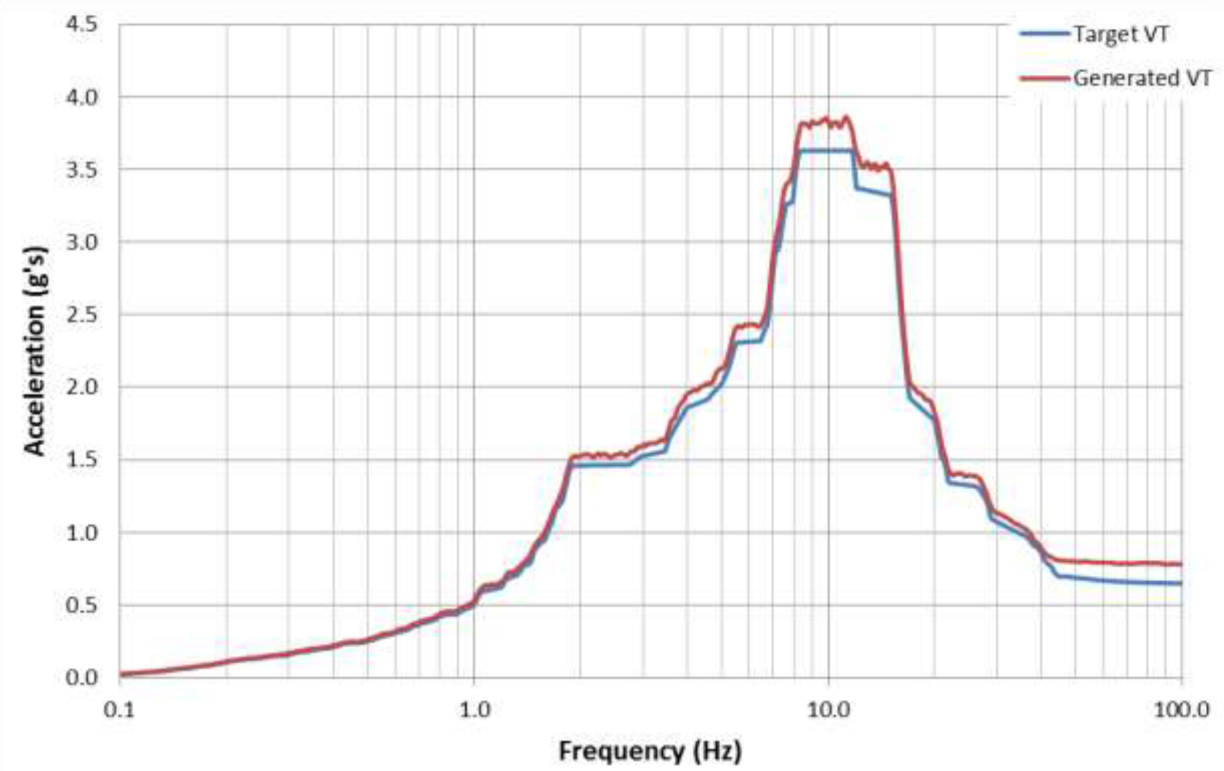

Figure 3-21 New Fuel Rack Vertical Average Generated Response Spectra

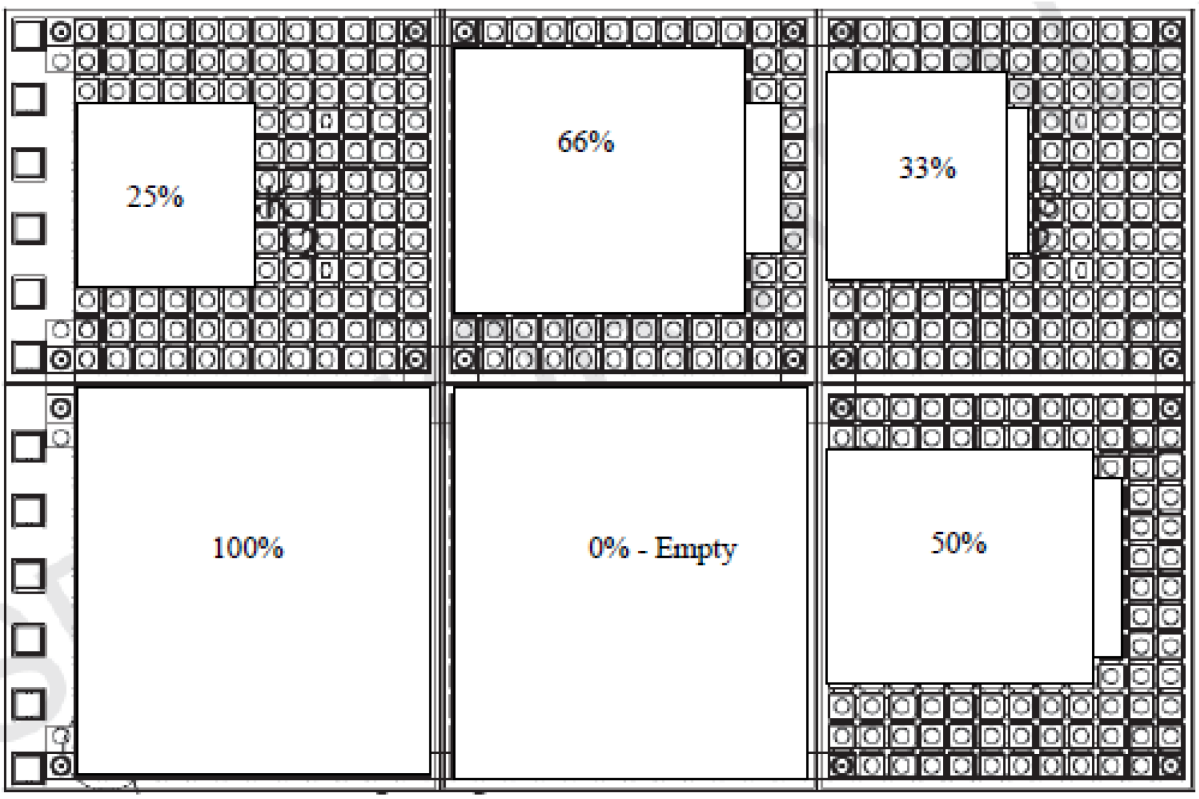

Figure 3-22 Fuel Loading Configuration

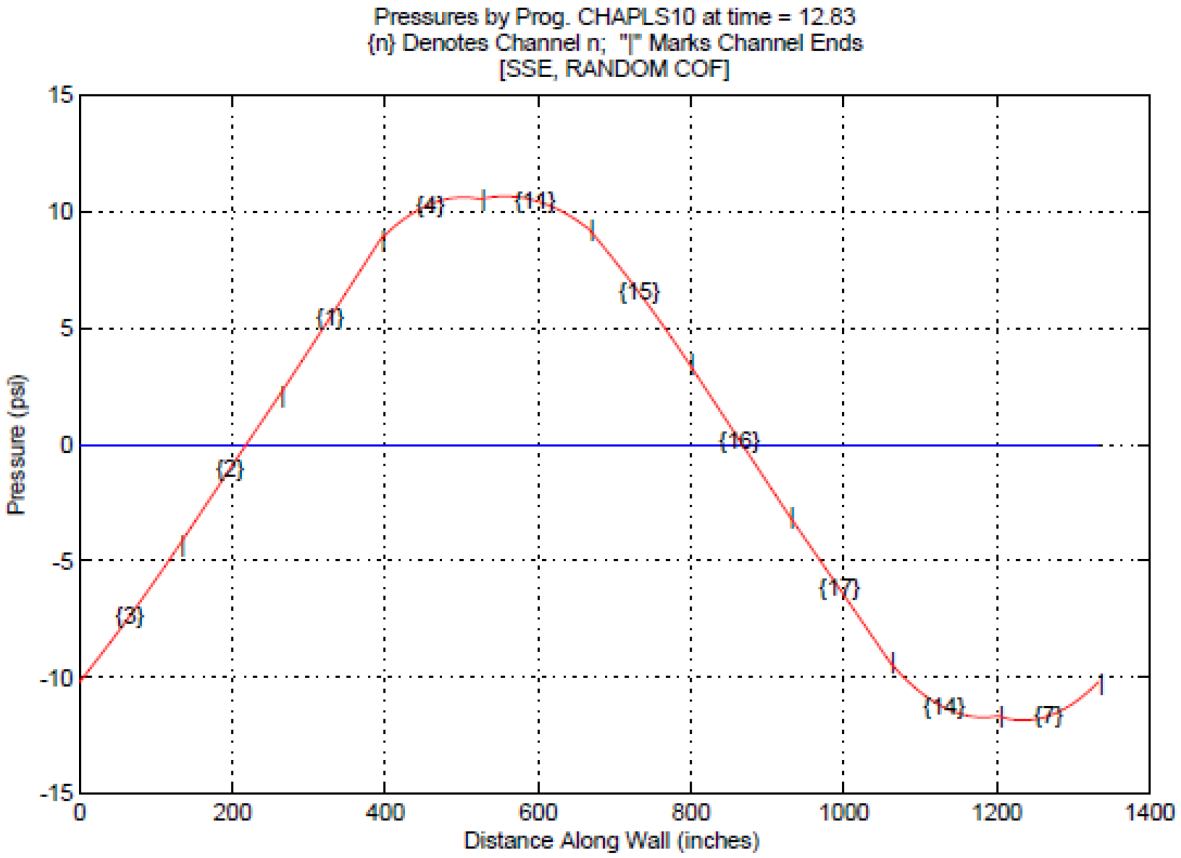

Figure 3-23 Hydrodynamic Pressure between the Spent Fuel Rack and the Spent Fuel Pit Wall

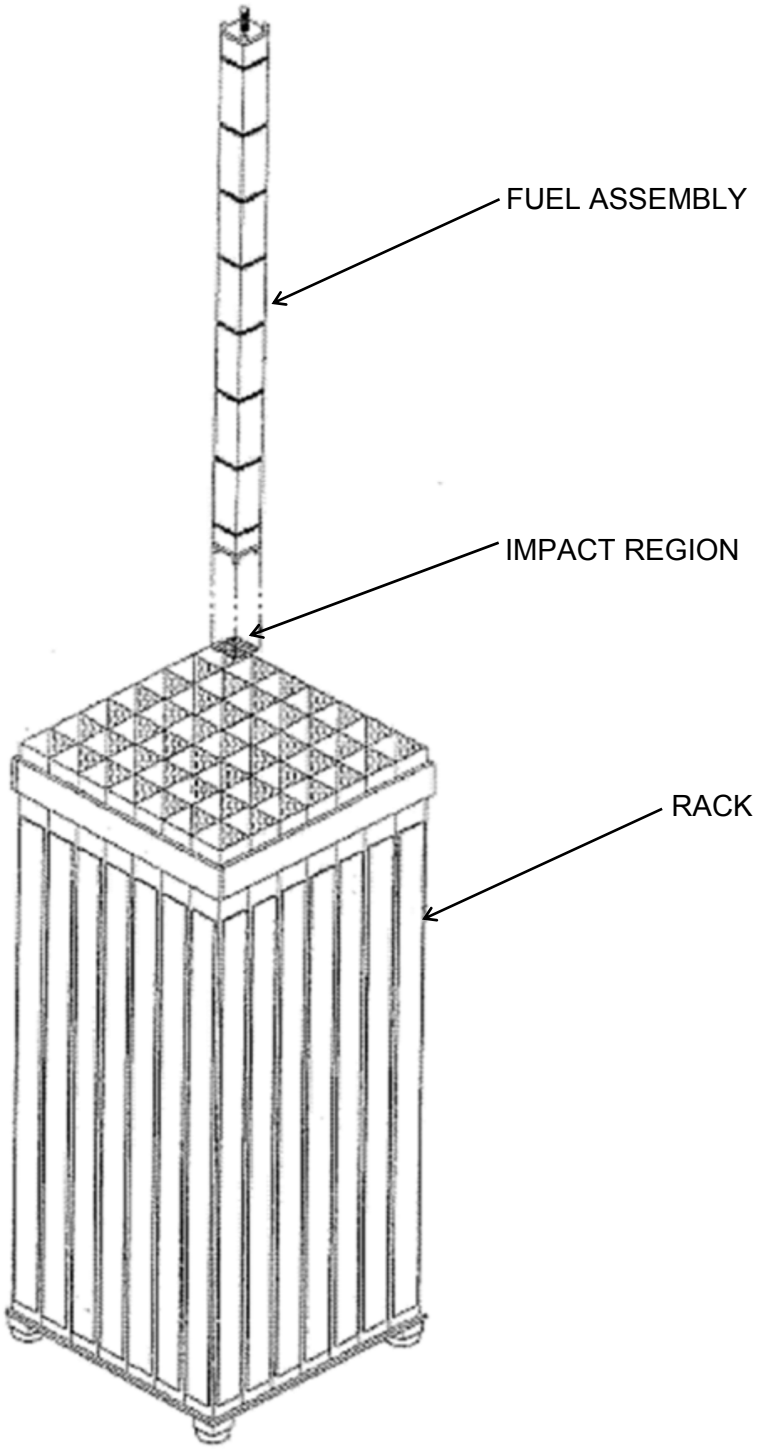

Figure 4-1 Schematic of the Straight Shallow Drop on a Rack Cell

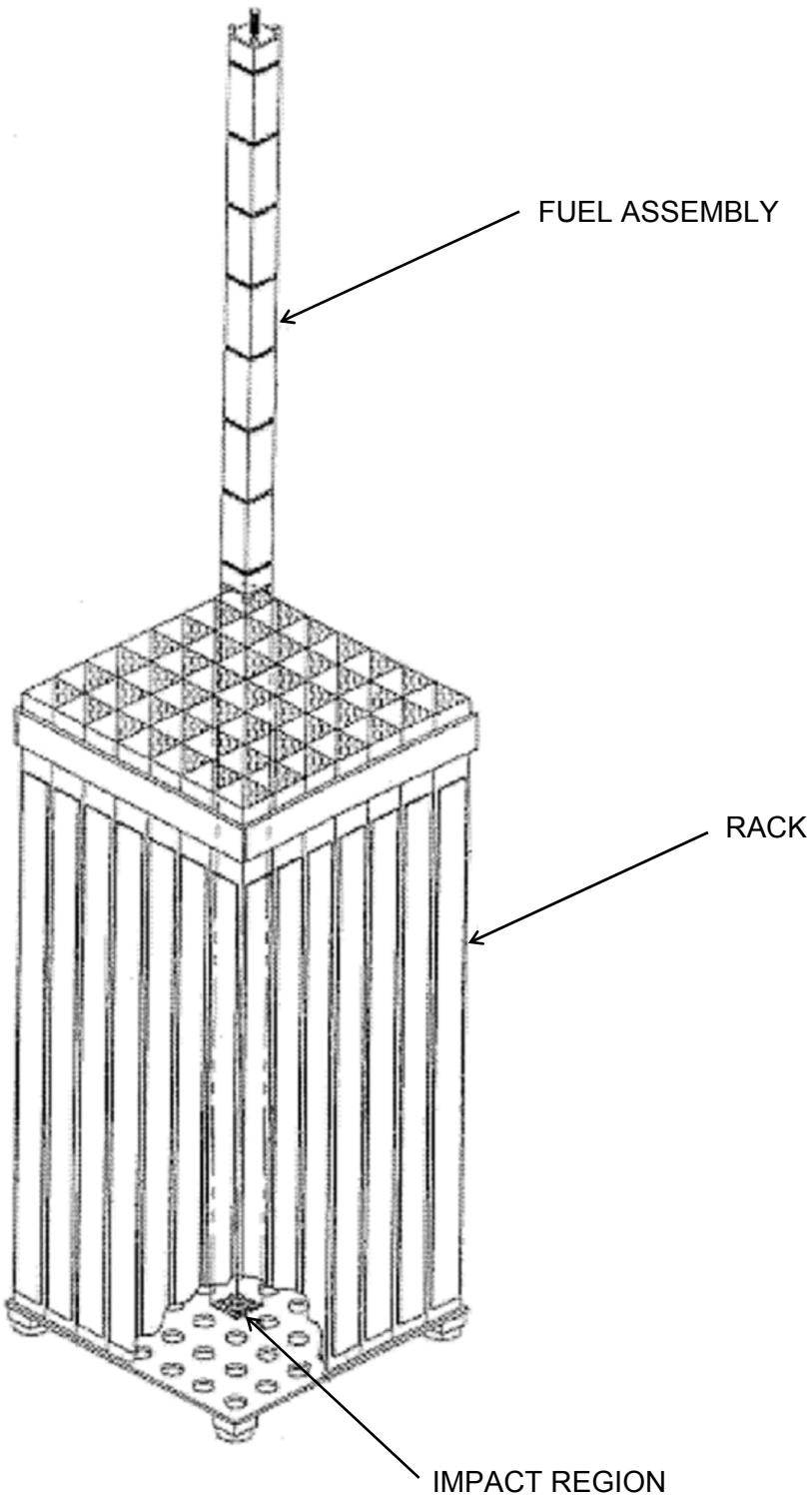

Figure 4-2 Schematic of the Deep Drop Scenario 1 on a Center Cell Location

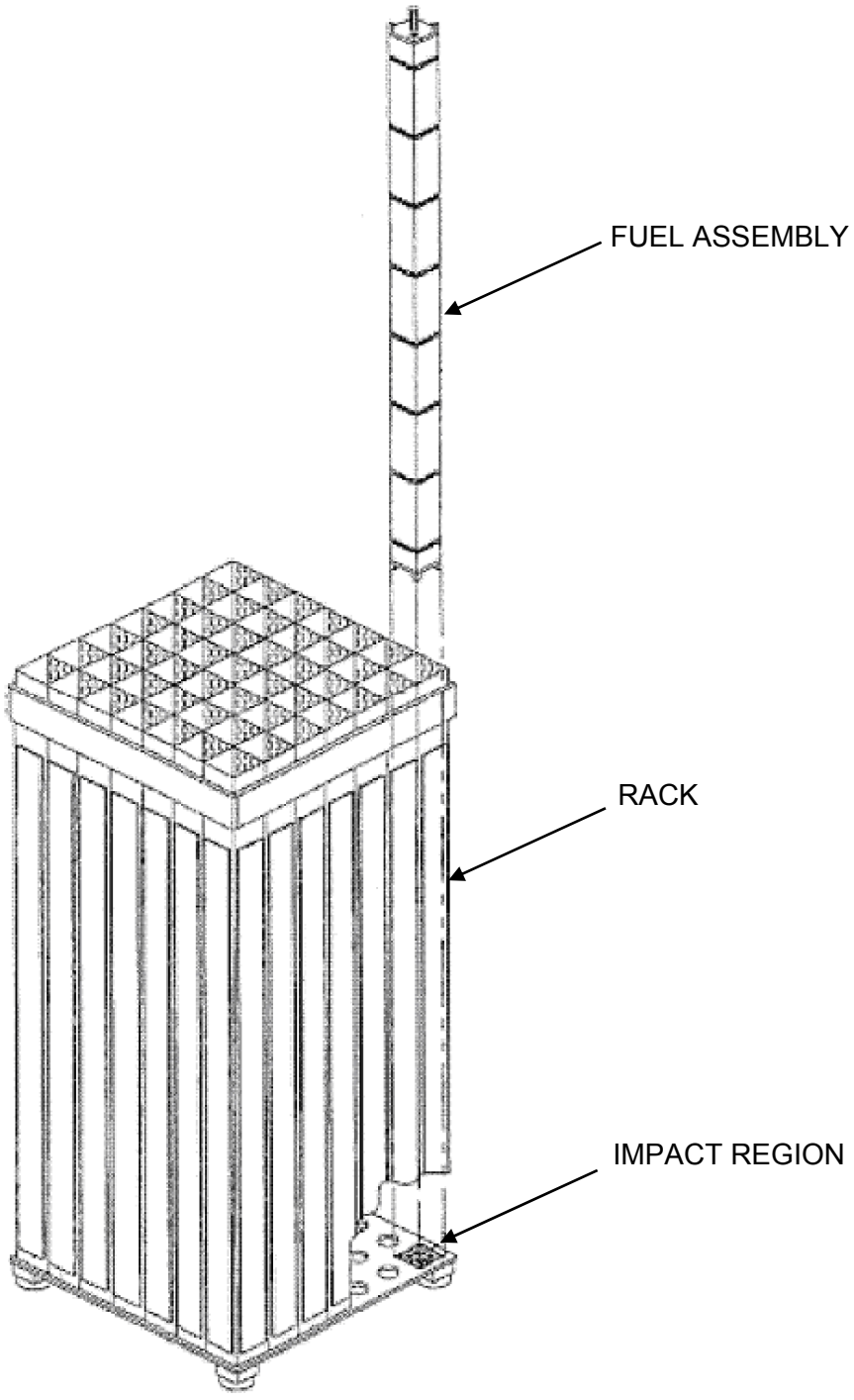

Figure 4-3 Schematic of the Deep Drop Scenario 2 on a Support Pedestal Location

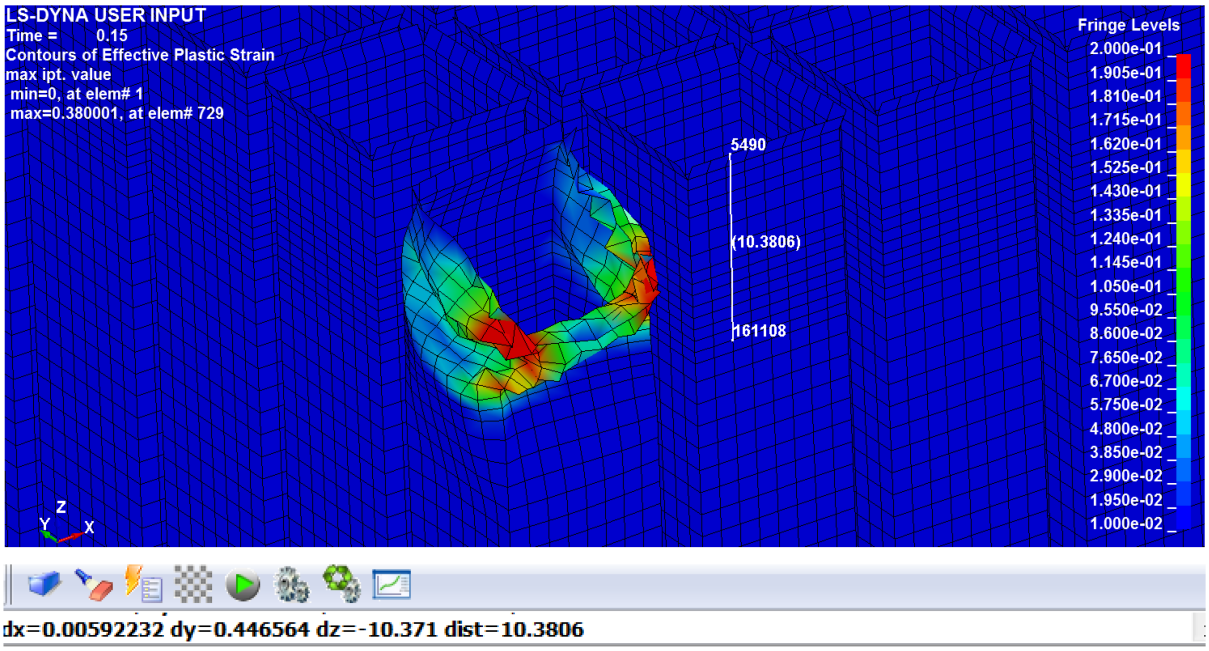

The vertical deformation (Z-dir.) of the rack cell is limited to 10.371 in. from the top of the rack

Figure 4-4 Plastic Strain and Deformation - Shallow Drop Analysis on SFR

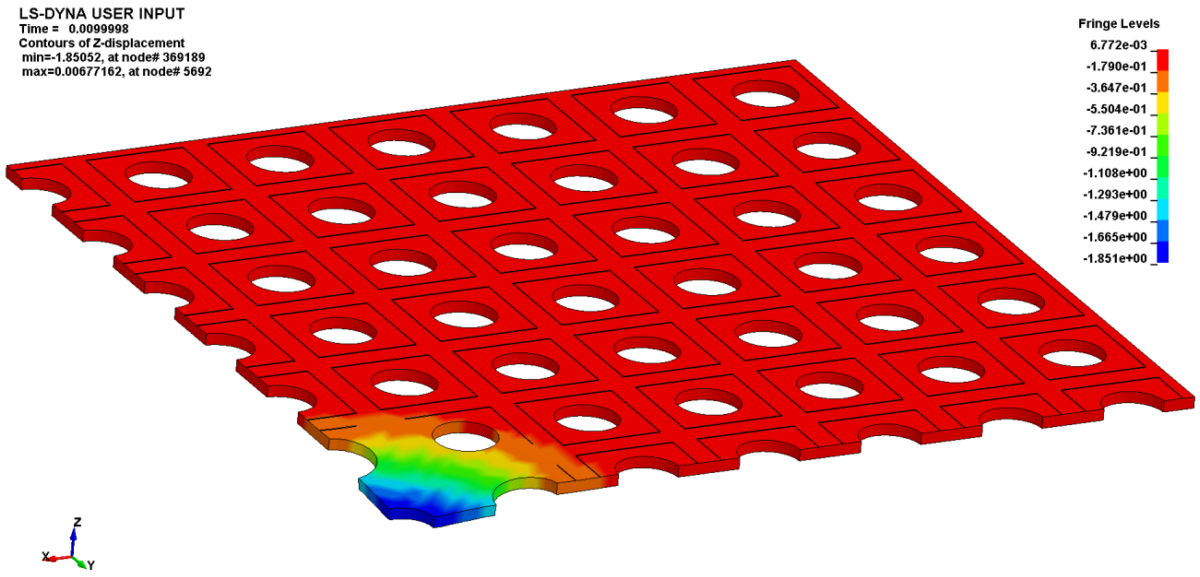

Figure 4-5 Baseplate Deformation - Deep Drop Scenario 1 on SFR